REPORT NVL-0059-005

[redacted]

STUDY OF ELECTRONIC TRANSPORT AND BREAKDOWN IN THIN INSULATING FILMS

Walter C. Johnson
PRINCETON UNIVERSITY
Department of Electrical Engineering
Princeton, New Jersey 08540
Telephone: (609) 452-4621

1 June 1977

SEMI-ANNUAL TECHNICAL REPORT NO. 3

Approved for public release; distribution unlimited.

Prepared for:

NIGHT VISION LABORATORY
U. S. Army Electronics Command
Fort Belvoir, Virginia 22060

Sponsored by:

DEFENSE ADVANCED RESEARCH PROJECTS AGENCY

DARPA Order No. 2182
Program Code. No. D10
Contract DAAG53-76-C-0059
Effective Date: 17 November 1975
Expiration Date: 17 November 1977

The views and conclusions contained in this document are those of the authors and should not be interpreted as necessarily representing the official policies, either expressed or implied, of the Defense Advanced Research Projects Agency of the U. S. Government.

Unclassified

SECURITY CLASSIFICATION OF THIS PAGE (When Data Entered)

REPORT DOCUMENTATION PAGE		READ INSTRUCTIONS BEFORE COMPLETING FORM
1. REPORT NUMBER NVL-0059-005	2. GOVT ACCESSION NO. AD-A129 102	3. RECIPIENT'S CATALOG NUMBER
4. TITLE (and Subtitle) STUDY OF ELECTRONIC TRANSPORT AND BREAKDOWN IN THIN INSULATING FILMS		5. TYPE OF REPORT & PERIOD COVERED — —
		6. PERFORMING ORG. REPORT NUMBER
7. AUTHOR(s) Walter C. Johnson Telephone: (609) 452-4621		8. CONTRACT OR GRANT NUMBER(s) DAAG53-76-C-0059
9. PERFORMING ORGANIZATION NAME AND ADDRESS Princeton University Department of Electrical Engineering Princeton, New Jersey 08450		10. PROGRAM ELEMENT, PROJECT, TASK AREA & WORK UNIT NUMBERS 61101E, ARPA 2182, D10, ~~024~~CJ
11. CONTROLLING OFFICE NAME AND ADDRESS Defense Advanced Research Projects Agency 1400 Wilson Boulevard Arlington, Virginia 22209		12. REPORT DATE 1 June 1977
		13. NUMBER OF PAGES 66
14. MONITORING AGENCY NAME & ADDRESS(if different from Controlling Office) Night Vision Laboratory DRSEL-NV-II Fort Belvoir, Virginia 22060		15. SECURITY CLASS. (of this report) Unclassified
		15a. DECLASSIFICATION/DOWNGRADING SCHEDULE

16. DISTRIBUTION STATEMENT (of this Report)

Approved for public release; distribution unlimited.

17. DISTRIBUTION STATEMENT (of the abstract entered in Block 20, if different from Report)

18. SUPPLEMENTARY NOTES

19. KEY WORDS (Continue on reverse side if necessary and identify by block number)

Insulating Films
Electronic Transport in Insulators
Charge Trapping in Insulators
Dielectric Breakdown
Silicon Dioxide

20. ABSTRACT (Continue on reverse side if necessary and identify by block number)

Recent progress is reported in an ongoing program of studies of high-field charge-carrier injection, transport, trapping, and dielectric breakdown in thin insulating films. The investigations reported here include the generation of interface states in the Si-SiO_2 system by ionizing radiation and by high-field stress, the high-field generation of electron traps in SiO_2, a method for measuring interface-state densities at low temperatures, and studies of high-field effects in the Al_2O_3-Si system.

DD FORM 1 JAN 73 1473 EDITION OF 1 NOV 65 IS OBSOLETE
S/N 0102-014-6601 |

Unclassified

SECURITY CLASSIFICATION OF THIS PAGE (When Data Entered)

TABLE OF CONTENTS

Page

1. INTRODUCTION

We report here on recent progress in an ongoing program of research directed toward a basic understanding of the electronic properties of thin insulating films and of the interfaces of such films with semiconductors and metals. Of particular interest are the high-field properties, including charge-carrier injection through the interfaces, electronic transport through the insulator, charge-carrier trapping and recombination at the interfaces and in the insulator, the high-field generation of interface states and trapping centers, and the mechanisms leading to dielectric breakdown. The objective of the program is to provide a rational basis for the choice of materials, processing methods and treatment of the insulating films in order to obtain the desired performance and reliability. The insulating films under study at the present time are silicon dioxide, aluminum oxide, and silicon nitride on silicon substrates. The techniques and apparatus that we have developed under this program are, moreover, immediately applicable to the study of other types of insulating films and substrates.

We have previously reported on many of the results of the studies made under this program,[1-29] and additional reports and papers are in preparation. The organization of this report is as follows:

The generation of interface states in the Si-SiO_2 system is a matter of great concern. In a previous report[25] we showed that after high-field stress at liquid nitrogen temperature, the interface states did not make their appearance until the sample had been warmed toward room temperature. In Ch. 2 of this report, J. J. Clement presents recent results obtained on radiation-induced interface states in the Si-SiO_2 system. By irradiation of the structure at 87°K, he finds that the nucleation of interface states is apparently associated with the presence of holes at the interface, but he finds further that even if the holes are annihilated by injecting electrons, the interface states appear when the sample is warmed. The interface states in his HCl-steam grown oxides are found to be generated in three temperature ranges: (1) near 140°K, (2) in the range 240-290°K, and (3) at approximately 333°K.

In Ch. 3, C. Jenq presents new results on high-field effects in the Si-SiO_2 system. He has previously reported[27] his observation that electron traps are created in SiO_2 at fields $\gtrsim$ 7 MV/cm, and in this report he gives his results on the rate of generation of the traps and on their capture cross sections. The high-field generation of electron traps may

have important consequences in short-channel IGFETS operating with large electric fields in the vicinity of the drain. In addition, Mr. Jenq gives recent results on the high-field generation of interface states, and he shows that electron photoinjection has an influence on interface-state generation. His techniques require the measurement of interface-state densities at liquid nitrogen temperatures, and for this purpose he has developed a low-temperature ledge (LTL) method for this measurement.

In Ch. 4, O. Bar-Gadda presents recent results obtained in a study of high-field effects in Al-Al_2O_3-Si structures. Electron trapping takes place near the negative electrode and positive charging takes place near the positive electrode, thus increasing the electric field in the central region of the insulator. Breakdown is observed to take place near the edge of the field plate, perhaps implying the importance of an edge effect.

In Ch. 5, S. S. Li gives the results of both corona and MIS studies of the Al_2O_3-Si structure. He confirms Mr. Bar-Gadda's observations of electron trapping near the negative electrode and positive charging near the positive electrode, and offers the results of photoinjection experiments to show that the concentration of electron traps is of the order of 10^{18} cm^{-3} and that the electron trapping cross section is approximately 3×10^{-13} cm^2. The observed positive charge is attributed to either hole injection from the positive electrode or field emission from neutral centers in the oxide rather than to impact ionization.

2. RADIATION-INDUCED INTERFACE-STATE FORMATION IN MOS CAPACITORS
(J. J. Clement collaborating)

2.1. Introduction

Previous investigations into the process of interface-state formation in MOS devices exposed to ionizing radiation have shown that the direct interaction of radiation at the Si-SiO_2 interface is not needed in order to produce interface states; however, interface-state formation is dependent on the transport of radiation-produced holes to the interface.[31,32] In one study, it was determined that the major part of the interface state generation occurs after the holes have had time to reach the interface.[33]

It has been shown by other workers that holes in thermally grown silicon dioxide are subject to a temperature-activated, field-dependent transport process through the oxide. Thus, at liquid nitrogen temperatures and for low values of applied electric field, the holes are essentially immobile and are trapped through the oxide near the point of creation.[34-41] However, it has been shown that the motion of holes through the oxide can be enhanced by applying higher electric fields and/or by illuminating the device with light having photon energies in the range from 1.6 to 2.0 eV.[40,41]

Although the transport of holes through thermally grown silicon dioxide has been studied at low temperatures, past studies of radiation-induced interface-state generation have been carried out almost exclusively at room temperature. In the investigation reported here, the irradiation of the MOS device was done at around 87°K, for several reasons. In addition to the intrinsic significance of how the interface-state density is affected by irradiation at this low temperature, we are better able to control the movement of the radiation-induced holes through the oxide to the Si-SiO_2 interface. Also, this procedure allows us to observe the effect of temperature on the interface-state formation process. As is shown in Sections 2.4 and 2.5 of this report, we find that irradiation of the MOS structure with soft X-rays produces negligible change in the number of interface states at 87°K. However, an increase in interface states is observed when the sample is subsequently warmed. This temperature effect is similar to the one that we reported previously for interface states generated in the Si-SiO_2 system by high fields.[25] We present evidence that only a temporary presence of holes at the interface is required to start the process of

interface-state generation. We observe that interface states are generated in this (HCl-steam) oxide in three temperature ranges: (1) near 140°K, accounting for approximately half of the interface-state generation; (2) in the range 240-290°K; and (3) at approximately 333°K. We suggest that the generation process is electrochemical in nature.

2.2. Description of Samples and Apparatus

The MOS capacitors used in these experiments had n-type (100) silicon substrates with 5-10 ohm-cm resistivity. On this an HCl-steam oxide was thermally grown at 875°C to a nominal thickness of 1000Å. Following a 10-minute anneal at 950°C in nitrogen, semi-transparent aluminum field plates were evaporated. The samples were fabricated at RCA Laboratories through the courtesy of K. M. Schlesier.

The sample was mounted on the cold finger of a vacuum cryostat, making it possible to cool the sample with liquid nitrogen. A resistive heater mounted on the sample stage allowed control of the temperature. The sample chamber was evacuated by an oil diffusion pump. The ionizing radiation used in these experiments was soft X-rays which were generated by 5 kV electrons strking a molybdenum target.

The sample chamber was fitted with a fused silica window for illumination of the sample. Ultra-violet light for the internal photoemission of electrons was provided by a Bausch and Lomb high-intensity monochromator with a Xenon lamp source. Light of lower energy was provided by a Bausch and Lomb tungsten-halide lamp source. Capacitance measurements were made with a Boonton model 72A capacitance meter operating at 1 MHz. Current measurements were made with a Keithley Model 610C electrometer.

2.3. Measurement of Interface-State Densities

Three methods of interface-state measurement were utilized in these experiments. At 333°K the technique utilizing the quasistatic C-V curve as described by Kuhn[42] and Castagne[43] was employed. At 87°K, a measure of the concentration of interface states in the central region of the bandgap was obtained by using the ledge phenomenon found in the low-temperature high-frequency C-V curves.[29,44-46] An example of this effect for a typical sample is shown in Fig. 2.1. In this figure, Curve A is the high-frequency C-V curve obtained at 87°K by ramping the bias from accumulation into deep depletion at a fairly fast rate (1 V/sec in this example). The sample is then

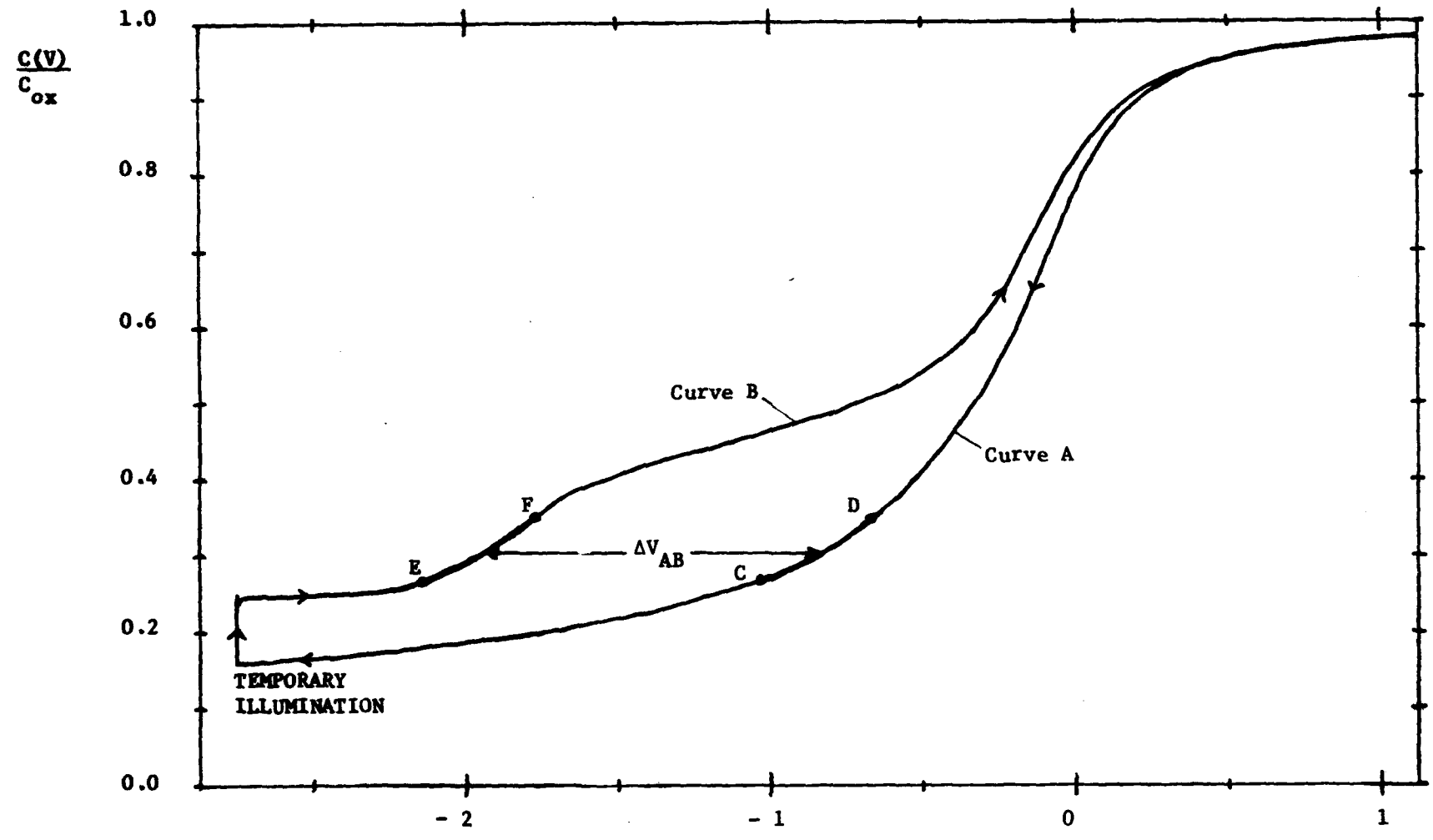

Fig. 2.1. Typical low-temperature high-frequency C-V curves for a fresh MOS capacitor used in this study. Curve A is the deep depletion curve obtained by ramping the bias from accumulation into deep depletion. After temporary illumination of the sample, ramping back up to accumulation results in curve B. The width of the ledge indicated by ΔV_{AB} is used to compute the number of interface states (Eq. 2.1).

temporarily illuminated with visible light, thus supplying minority carriers to fill the interface states. Following this, the bias is ramped toward accumulation, resulting in Curve B. The ledge present in this curve is due to majority carriers filling the interface states in the central region of the bandgap. As is shown in Sec. 3.2 of this report, the section EF of Curve B is essentially parallel to the section CD of Curve A, and the voltage difference, ΔV_{AB}, between the two curves in this region can be used to determine the number of interface states in the central portion of the bandgap according to the formula:

$$N_i = C_{ox}\Delta V_{AB}/q \qquad (cm^{-2}) \qquad (2.1)$$

where C_{ox} is the oxide capacitance per cm^2 and q is the magnitude of the electronic charge. As is also shown in Sec. 3.2 of this report, the central region of the bandgap in which the interface states make the transition at $90^{\circ}K$ is approximately 0.7 eV wide in silicon, and so the average concentration of interface states in $cm^{-2}eV^{-1}$ in this central bandgap region is obtained by dividing N_i (cm^{-2}) by 0.7 eV.

The Gray-Brown shift of the flatband voltage[47] as the sample is cooled below room temperature provides another method for measuring the number of interface states present in the upper part of the band gap.

The foregoing three methods complement each other and in addition they serve to check each other in their regions of overlap.

2.4. Influence of Holes and Temperature on Interface-State Formation

We have reported previously[25] that if an Si-SiO_2 structure is subjected to high field stress at low temperature ($91^{\circ}K$), the generation of interface states is observed only after the sample has been warmed toward room temperature. It is well known that if an MOS structure is exposed to ionizing radiation, the buildup of trapped holes is accompanied by an increase in interface-state density. The purpose of these experiments was to examine further the connection between the trapped holes and the interface states. For this purpose we used soft X-rays to produce hole-electron pairs in the oxide at $87^{\circ}K$, following which the electrons were drifted out by application of a moderate electric field, leaving the holes behind. The holes could then be transported to one interface or the other by means of a

larger electric field together with excitation by visible light. The holes were then annihilated by photoinjected electrons, after which the sample was warmed to observe the generation of interface states. The results of these experiments are summarized in Table I, as follows:

Column I identifies the sample. A fresh sample was used each time. All fresh samples were essentially identical.

Column II shows the number of interface states, N_i cm^{-2}, as determined on the fresh sample at 87°K by the low-temperature ledge method, using Eq. 2.1.

Column III shows the gate voltage used during a 20-minute irradiation with soft X-rays at 87°K. This bias will quickly drift the radiation-produced electrons to the positive electrode but will produce very little transport of holes in the oxide at this temperature. Some of the holes produced in the thin hole-trapping layer near the Si-SiO_2 interface may be trapped there. Also, the holes produced in the bulk of the SiO_2 will have some initial motion[48] before they are immobilized, and with a positive gate bias this motion will bring some holes into the hole-trapping region. With a negative gate bias, some of the radiation-produced holes in the substrate may drift into the interfacial region. Thus we expect some trapping of holes near the interface for either polarity of gate voltage, but, at these fields, and without light assistance, the main body of holes in the bulk will be essentially immobile at 87°K.

Column IV shows the gate bias which was applied for three hours at 87°K to transport the radiation-produced holes through the bulk of the oxide. The transport of holes during this period was assisted by illuminating the sample with tungsten light which was filtered through a water cell and a yellow filter. After drift of the holes through the bulk of the oxide, essentially all of the holes, both those remaining in the bulk and those trapped at the interface, were annihilated by an internal photoinjection of electrons at 87°K.

I	II	III	IV	V	VI	VII
SAMPLE	N_i (CM^{-2}) INITIAL	V_G DURING IRRADIATION	V_G BIAS FOR 3 HR.	N_i BEFORE WARM-UP	N_i AFTER WARM-UP	ΔN_i (CM^{-2}) (COL. VI - COL. II)
1	2.31×10^{11}	NO X-RAY	+ 35 V	2.31×10^{11}	2.38×10^{11}	$(0.65 \pm 0.5) \times 10^{10}$
2	2.55×10^{11}	+ 15 V	NO BIAS TREATMENT	2.55×10^{11}	2.76×10^{11}	$(2.1 \pm 0.5) \times 10^{10}$
3	2.47×10^{11}	- 15 V	- 35 V	2.47×10^{11}	2.75×10^{11}	$(2.8 \pm 0.5) \times 10^{10}$
4	2.39×10^{11}	+ 15 V	+ 35 V	2.44×10^{11}	3.03×10^{11}	$(6.4 \pm 0.5) \times 10^{10}$

Table I. Radiation-induced generation of interface states. (See text for explanation)

UV light with a photon energy of approximately 5 eV was used for this purpose.

Column V shows the density of interface states at 87°K after the foregoing processes had been completed. Comparison with Col. I shows that the number of interface states remained essentially unchanged throughout the operations of X-irradiation, drift of most of the holes to one interface or the other, and subsequent annihilation of the holes.

Column VI shows the effect of warming the sample and holding it at room temperature for approximately 12 hrs, after which the sample was again cooled to 87°K so that a direct comparison of N_i could be made using the same technique as before.

Column VIII shows the increase in interface states that resulted from each of the four sequences of operations.

We can make the following observations from the results shown in Table I. Firstly, from Col. V we see that none of the sequences resulted in an appreciable increase in interface states so long as the sample was held at 87°K. The interface states appeared only during or after warmup. Secondly, the four different sequences show appreciable differences in Col.VII, as follows: On Sample 1, which had no X-irradiation and served as a control sample, the increase in N_i after warming was so small as to be negligible. On Sample 2, which was irradiated with positive gate bias but which had no subsequent drift of holes to either interface, the increase in interface states was a moderate one which might have been associated with holes that were produced near the interface and trapped there. On Sample 3, where the holes produced in the bulk were transported to the gate, the increase in interface states was similarly moderate in value. The difference between Samples 2 and 3 is within experimental error and may not be significant. On Sample 4, however, where the holes in the bulk were transported to the interface, the increase in interface states is quite appreciably greater.

Thus the generation of interface states appears to be associated with holes at the interface, and the states do not make their appearance until the sample is warmed. However, since the holes were annihilated before the sample was warmed, merely the temporary presence of holes at the interface appears to be sufficient to start the interface-state generation process.

2.5. Temperature Dependence of the Interface-State Formation

In order to obtain information on the temperature dependence of the interface-state formation process, the following experiment was performed. An MOS capacitor sample was cooled to 87°K and, with the gate biased at +20 V, was exposed to soft X-rays for 30 minutes. The sample, with its temperature held at 87°K, was then biased at +35 V for 3 hours while illuminated with light from a tungsten lamp filtered through a water cell and a yellow filter. As described previously, this procedure transports the holes through the bulk of the oxide to the $Si-SiO_2$ interface. Following this, electrons were photoinjected into the oxide to recombine with the remaining holes. The sample was next warmed to a particular temperature and held there for one hour, then it was cooled to 87°K and the width of the ledge of the low-temperature high-frequency C-V curve was measured for computation of N_i (Eq. 2.1). The sample was heated (and cooled to 87°K) in successive steps to temperatures of 120, 140, 160, 190, 220, 240, 262, 290, 333°K. The total increase in the number of interface states following the last step was 7.1×10^{10} cm^{-2} as computed from the net change in the width of the ledge. The percentage of this increase which was observed following each step is shown in Fig. 2.2. There appear to be three peaks of interface-state generation, one near 140°K, a broad peak centered at about 270°K, and a third peak at 333°K. It is interesting to note that the peak below 160°K accounts for approximately half of the increase in interface states and that the peaks above 220°K account for the remaining half.

2.6. Summary

1) MOS capacitors exposed to ionizing radiation at 87°K show negligible interface generation for periods up to 3 hrs.

2) Upon warming, interface states are formed. In our HCl-steam grown samples, approximately half of the states are formed near 140°K. The remainder are generated in two temperature ranges: from 240-290°K, and near 333°K.

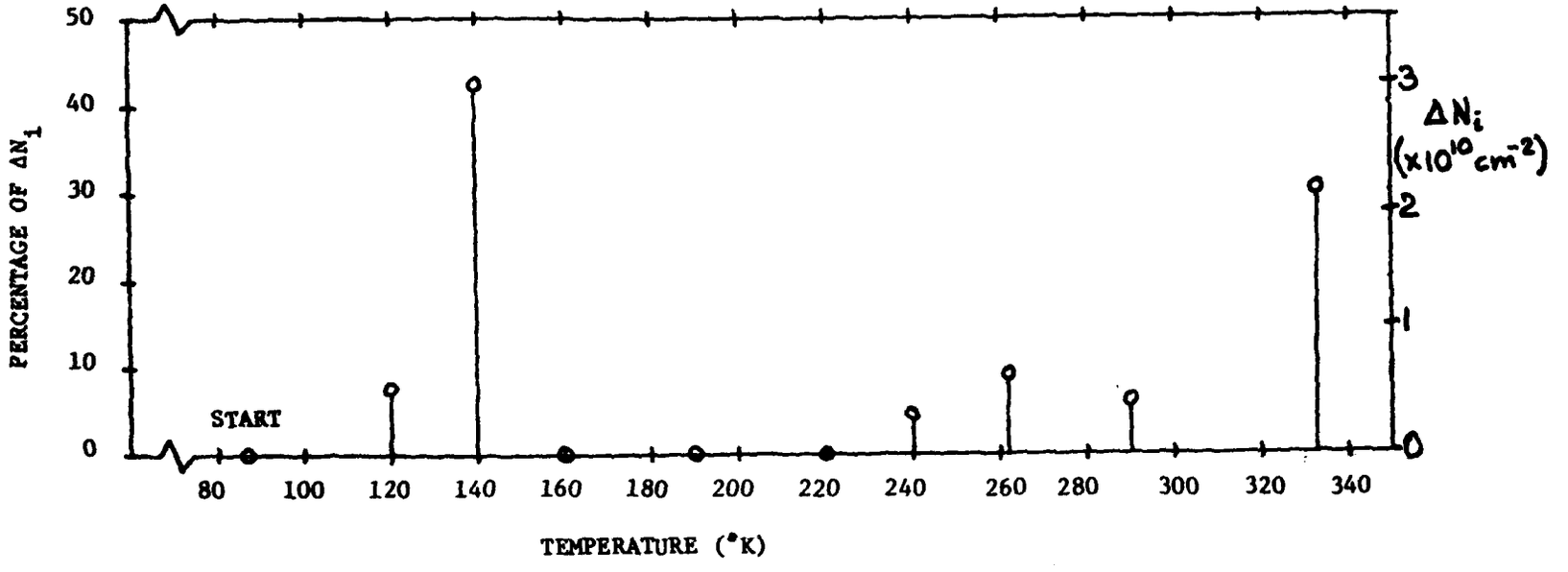

Fig. 2.2. Generation of interface states vs. temperature after exposure to soft X-rays at 87°K. The sample was (a) heated to 120°K, held for 1 hr, then cooled to 87°K for measurement of interface-state density by the ledge method; (b) heated to 140°K, held for 1 hr, then cooled to 87°K for measurement of interface-state density; and similarly for the successively higher temperatures shown by the circles.

3) The interface-state generation takes place despite the fact that the holes, with which their nucleation appears to be associated, had been annihilated by recombination with photoinjected electrons before the warmup process was initiated.

The requirement of thermal energy for the formation of the interface states suggests that the phenomenon may not be purely electronic but may be electrochemical in nature. Some suggestions in this regard have been made by C. T. Sah.[48]

3. A STUDY OF HIGH-FIELD EFFECTS ON MOS CAPACITORS
(C. Jenq collaborating)

3.1. Introduction

In this chapter we present the results of a further study of the effects of high-field stress on MOS capacitors. Our techniques require the use of liquid-nitrogen temperatures where the conventional methods of determining interface-state densities can not be employed. In Sec. 3.2 we present a method that we have developed for overcoming this difficulty. In the final sections, 3.3 - 3.5, we describe our recent results on the high-field generation of interface states and of bulk electron traps in the $Si-SiO_2$ system.

3.2. Low-Temperature Ledge (LTL) Technique for Measuring Interface-State Densities

The usual methods for measuring interface-state densities require the charge in the interface states to be in equilibrium with the applied voltage, and this condition can not be achieved within reasonable amounts of time at lowered temperatures. Brown and Gray[50] observed a ledge phenomenon in the C-V curves at liquid-nitrogen temperatures which they attributed to the presence of interface states, and Goetzberger and Irwin[51] related the width of the ledge to the density of interface states in the central region of the bandgap. We have analyzed the effect in greater detail and have made use of the phenomenon in our low-temperature studies of interface states. The low-temperature ledge (LTL) method is analyzed and described in the following paragraphs.

Figure 3.1 shows the C-V curves of a MOS capacitor measured at 91°K (curves 1 and 2) and an ideal deep-depletion C-V curve calculated for the temperature of 91°K (curve 3). Curve 1 was taken by sweeping the bias at -1.0V/sec from accumulation into deep-depletion in the dark. At Point A the sample was illuminated with visible light to generate minority carriers. This caused the capacitance to increase to Point B. The light was cut off, whereupon the capacitance dropped to Point C. The gate voltage was then ramped up at 1.0V/sec, producing Curve 2.[51] From now on we shall call Curve 1 the deep-depletion curve and Curve 2 the light-assisted curve. The

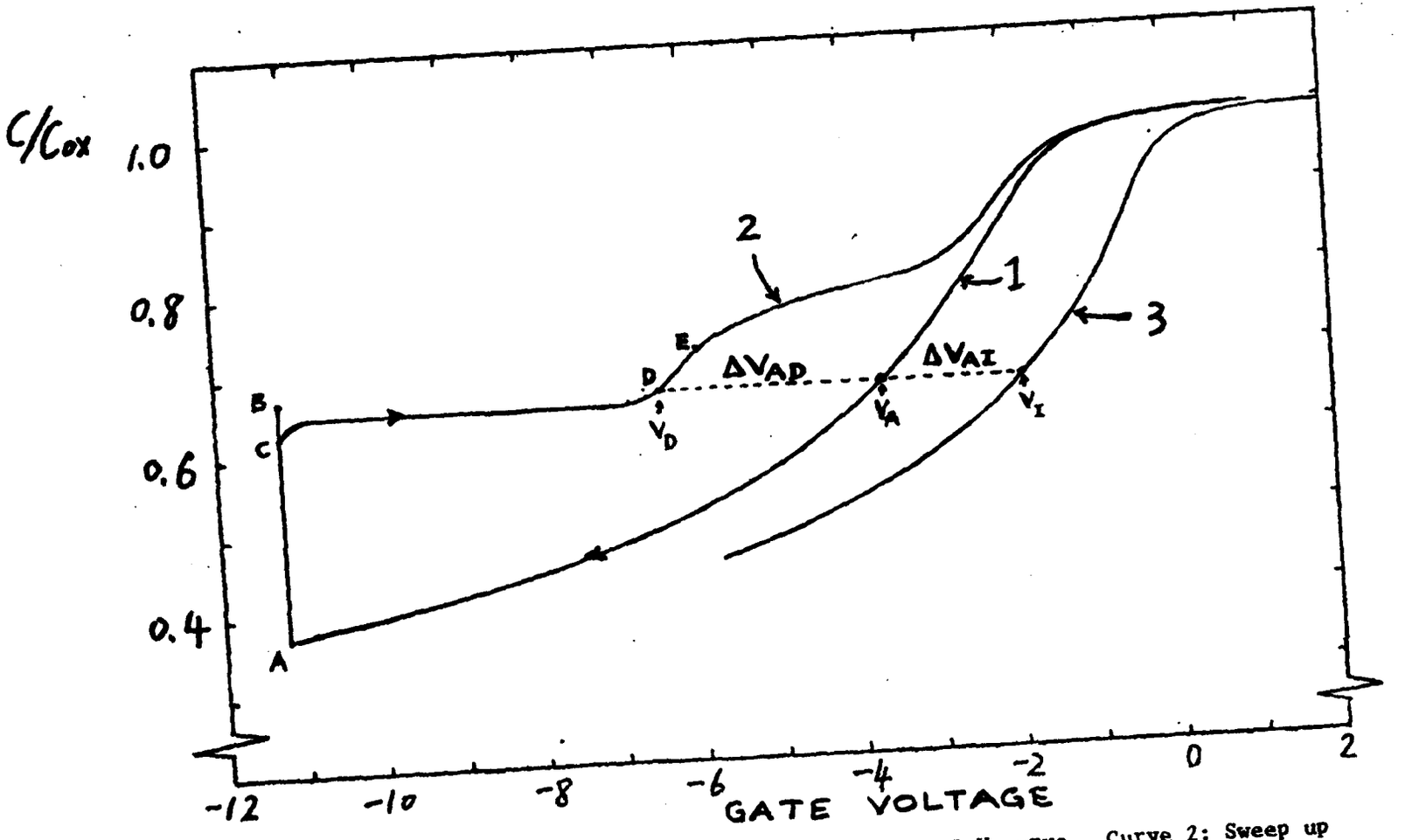

Fig. 3.1. C-V curves at 90°K. Curve 1: Deep-depletion C-V curve. Curve 2: Sweep up after temporary illumination. Curve 3: Ideal deep-depletion C-V curve.

features of the curves will be explained in the following paragraphs.

The emission time constant for an electron captured by an interface state with an energy level E_s is given by[52]

$$\tau_{en} = \frac{1}{v_{th}\sigma n_i} \exp(E_i - E_s)/kT$$

where v_{th} is the thermal velocity electrons, σ is the electronic capture cross section, n_i is the intrinsic carrier density, and E_i is the intrinsic level of the semiconductor. At 90°K, by taking σ to be 10^{-15} cm^2 and v_{th} to be 10^7cm/sec, τ_{en} is found to be 0.1, 1, 10, 100 and 1000 sec when the interface state is at 0.18, 0.19, 0.21, 0.23 and 0.24 eV below the conduction band, respectively. Hence a slight change of 0.01 eV in the energy level of the interface state will result in a change of τ_{en} of an order of magnitude. During the period when the deep-depletion curve (Curve 1 in Fig. 1) was taken, we may then assume that the electrons which occupied the interface states with an energy level 0.20 eV or more away from the conduction band edge would not be emitted into the conduction, while if the interface state was within 0.20 eV the electrons would have time to be emitted from the states. Note that this approximation will result in an error of not more than 0.02 eV. The possibility that the interface states can capture holes is unlikely due to the negligible generation rate of holes at 90°K.

Thus the electrons which are captured by the interface states with energy levels greater than 0.20 eV away from the conduction band will be frozen in the states. If the capacitor is laterally uniform, the part of the C-V curve below this point should be parallel to the ideal deep-depletion curve.[21] The voltage shift $\Delta V_{AI} = V_A - V_I$ between the lower part of the two curves is due to the oxide charges plus the charges frozen into the interface states. The states which are more than 0.20 eV away from the conduction band edge will remain in their more negative state, and those closer than 0.20 eV will be in their more positive state owing to their emission of electrons. Let N_{sa} be the total number of acceptor-type interface states which are 0.20 eV away from both the conduction and the valence band edges, N_{sav} be those which are within 0.20 eV of the valence band edge, and N_{sdc} be the total number of donor-type interface states that are within 0.20 eV of the conduction band edge. Also, let Q_{ox} denote the

equivalent oxide charge (referred to as the SiO_2-Si interface). Then, we have from the above discussion,

$$\Delta V_{AI} = V_A - V_I = q \frac{d_{ox}}{\varepsilon_{ox}} \left(\frac{-Q_{ox}}{q} + N_{sa} + N_{sav} - N_{sdc} \right) \tag{3.1}$$

where d_{ox} is the oxide thickness, ε_{ox} is the dielectric permittivity of the oxide, and q is the magnitude of the electronic charge.

In the case of the light-assisted curve before the sample is ramped up (Point C of Fig. 1), the SiO_2-Si interface region is flooded with holes generated by the light. The interface states are then all occupied by holes. When the gate voltage is swept toward accumulation, the capacitance remains almost constant at a magnitude higher than the thermal equilibrium value because of the presence of the excess holes at the interface. The constancy of the capacitance indicates that the width of the depletion layer has remained constant. The external charging current during this period is caused by the reduction of the excess holes in the interface region. The reduction process can be either the recombination of the excess holes with the electrons in the conduction band through the assistance of the bulk traps or the interface states, or the diffusion of the holes out of the depletion layer. With a sweep rate of 1 V/sec, the recombination current was calculated to be at least 12 orders of magnitude less than the charging current $C_{ox} \frac{dV_G}{dt}$. Hence, these excess holes diffuse out of the interface region at a rate determined by the ramping speed. When the number of holes remaining is negligible, the depletion layer then starts to respond to the change of gate voltage and the capacitance begins to increase (Point D) as a consequence of the reduction of the depletion width. As the capacitance increases, the surface potential is reduced and the electron concentration in the conduction band is increased. Eventually at Point E the recombination current[51] from the electrons in the conduction band and the holes in the interface states is large enough to dominate the charging current. The section between Points D and E of Curve 2 will then be parallel to the corresponding section of the ideal deep-depletion curve, provided the sample is uniform. Here the voltage shift $\Delta V_{DI} = V_D - V_I$ between the two sections of curves is due to the oxide charge and the changes in interface state charge. For those states which are more than 0.20 eV above the valence band, the holes previously captured will be frozen in, while the states that are

within 0.20 eV from the valence band edge will be in their more negative state owing to the emission of holes. Let N_{sd} denote the number of donor-type states which are more than 0.20 eV away from both the conduction and valence bands, N_{sdc} denote those within 0.20 eV from the conduction band, and N_{sav} denote the acceptor-type states within 0.20 eV from the valence band. Then we have:

$$\Delta V_{DI} = V_D - V_I = q \frac{d_{ox}}{\varepsilon_{ox}} \left(\frac{-Q_{ox}}{q} - N_{sd} - N_{sdc} + N_{sav} \right) \tag{3.2}$$

From Eqs. (3.1) and (3.2) we have

$$\Delta V_{AD} = V_A - V_D = q \frac{d_{ox}}{\varepsilon_{ox}} (N_{sa} + N_{sd}) \tag{3.3}$$

or

$$N_{sa} + N_{sd} = \frac{1}{q} \frac{\varepsilon_{ox}}{d_{ox}} \Delta V_{AD} \tag{3.4}$$

Equation (3.4) gives the interface-state density in cm^{-2} for those states which are 0.20 eV away from both the conduction valence bands, i.e., in the mid 0.7 eV of the band gap. Goetzberger and Irwin[51] and Gray[46] first observed the possibility of using the ledge of the light-assisted curve to measure the interface state density, but the ledge was not unambiguously defined.

For a MOS capacitor biased in the regime where the change in the capacitance is due solely to the change of the depletion capacitance of the substrate, we have the following relationship (for a n-type sample):

$$\left(\frac{C_{ox}}{C} \right)^2 = 1 - \left(\frac{2 C_{ox}^2}{q N_D \varepsilon_s} \right) (V_G - \Delta V) \tag{3.5}$$

where C_{ox} is the oxide capacitance, N_D is the donor concentration, ε_s is the dielectric permittivity of the substrate, V_G is the gate voltage, and ΔV is the voltage shift due to the combination of metal-semiconductor work-function difference, oxide change, and interface-state change.

If $(\frac{C_{ox}}{C})^2$ is plotted against V_G for the lower part of Curve 1 and the section between D and E of Curve 2, then two parallel straight lines with

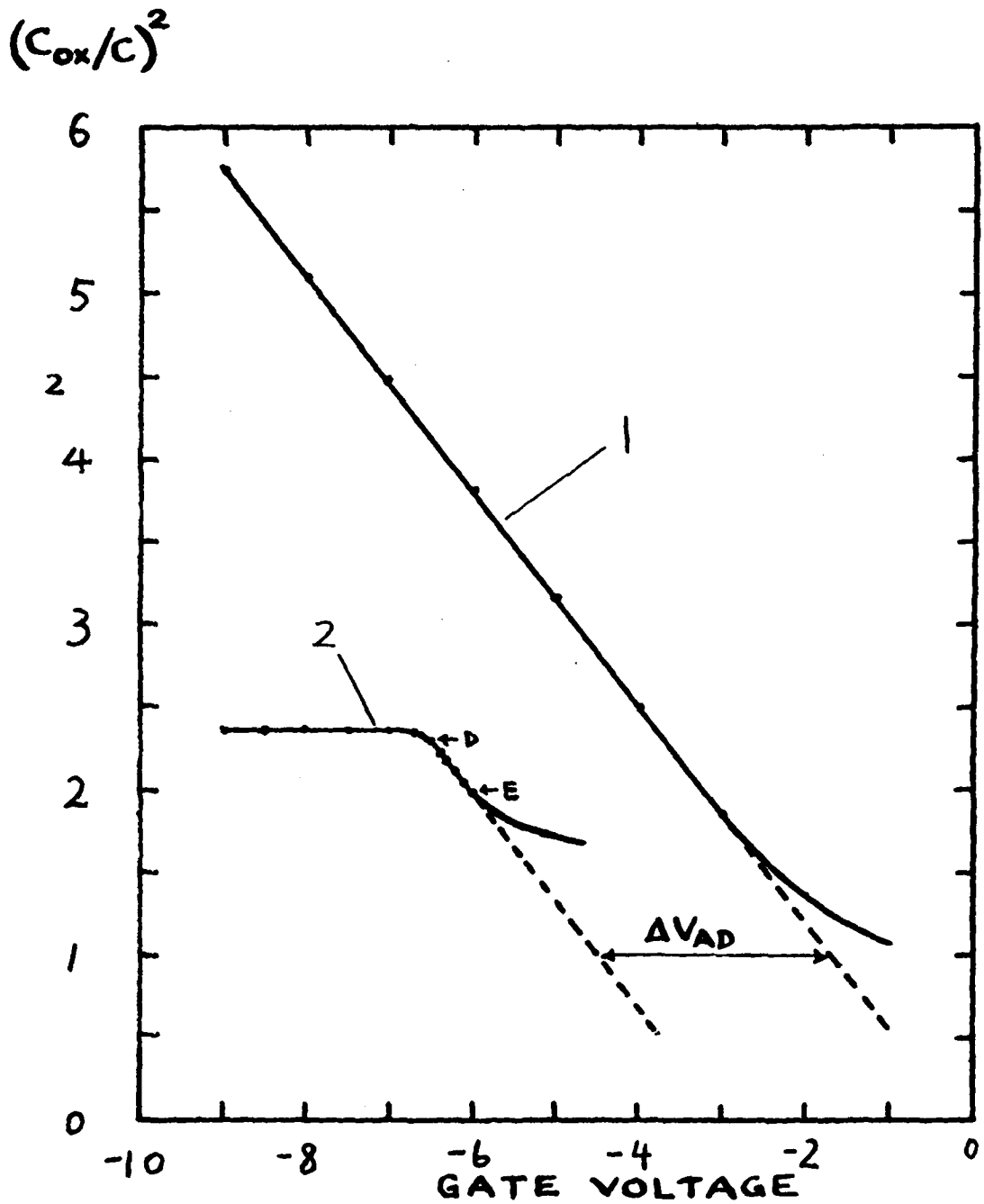

Fig. 3.2. Plot of $(C_{ox}/C)^2$ vs. gate voltage for the sample of Fig. 3.1. The solid parts of Curves 1 and 2 correspond to Curves 1 and 2 of Fig. 3.1.

the same slope should be obtained as in Fig. 3.2. The displacement between the two lines offers an alternate way of determining ΔV_{AD} for use in Eq. (3.4).

3.3. Generation of Interface States at 90°K During Internal Photoinjection After High-Field Stress.

3.3(A). Introduction

As was described in the last report,[27] electron traps, not initially present, were found to exist in the oxide layers of MOS capacitors after the samples had been subjected to high-field stress. It was also found that if two samples were subjected to the same high-field treatment at low temperature but received different quantities of photoinjected electrons (so that one sample had more field electron traps than the other), the two still showed essentially the same amount of interface-state generation after they had been warmed up to room temperature. We still find this to be a valid, reproducible result; however, more recently, we have also observed that if the interface-state density is measured by the LTL method before warming the sample, additional interface states, apparently related to the photoinjection of electrons, are indicated by the test. This phenomenon is discussed in the following section.

3.3(B). Experimental Evidence

The samples used in the following discussion were RCA HCl-steam grown SiO_2 films on (100) Si substrates with 5-10 Ωcm resistivity. The gates were semi-transparent aluminum.

Figure 3.3 shows three sets of curves. Set 1 consists of the initial 90°K deep-depletion curve and the light-assisted curve of the fresh sample. Set 2 is a similar set of curves taken after high-field stress, with field plate positive, at 7.4 MV/cm for 30 min at 90°K, and Set 3 are the curves taken after internal photoinjection from the Si substrate at an interface field of approximately 1.0 MV/cm for 3 hrs. The initial interface-state density in the mid 0.7 eV region of the bandgap is 2.52×10^{11} cm^{-2} calculated by the LTL method. The deep-depletion curve in Set 2 is slightly distorted, but the distance between the deep-depletion and the light-assisted curves remains approximately the same, and the interface-state density is

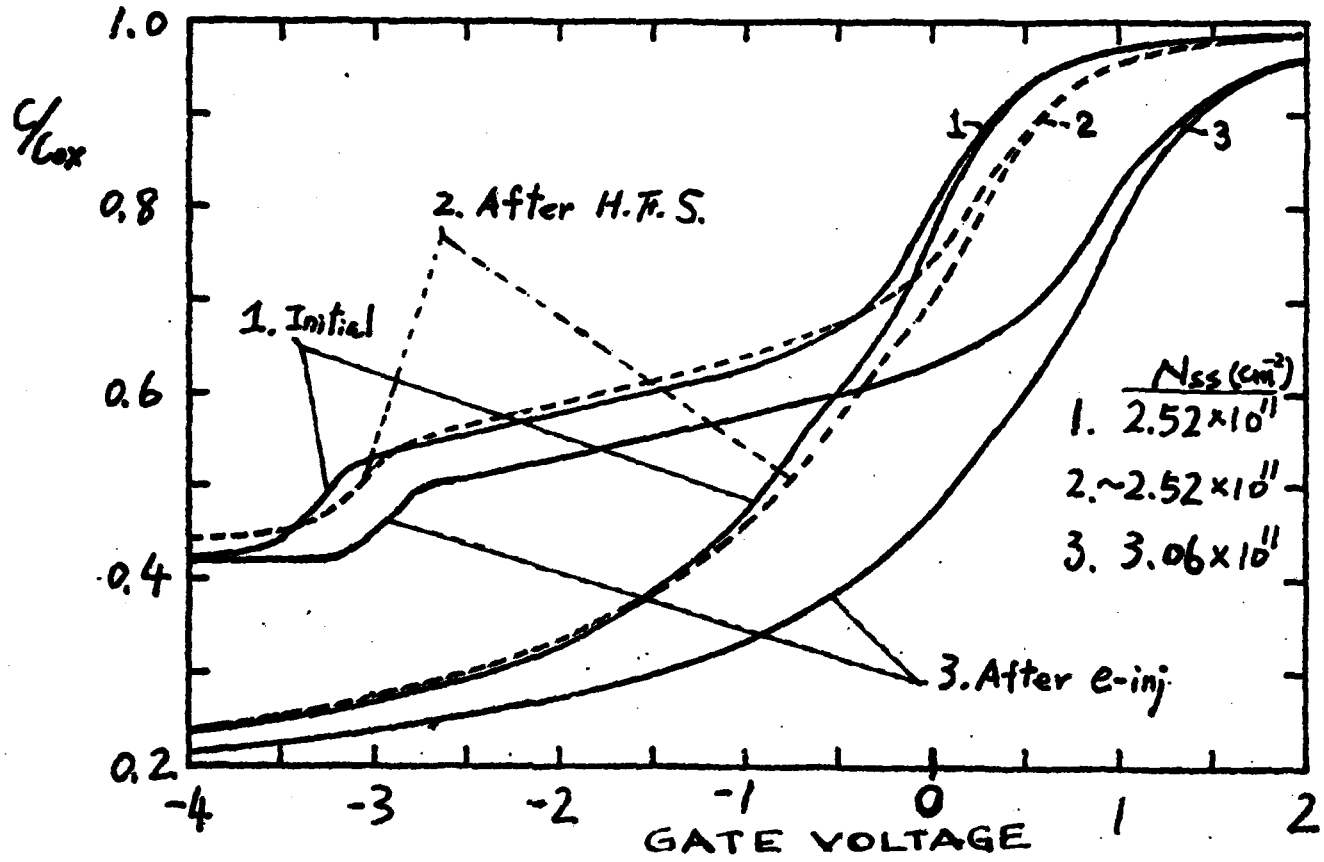

Fig. 3.3. C-V curves taken at 90°K. Set 1: Initial curves. Set 2: After high-field stress at 90°K. Set 3: After internal photoinjection at 90°K.

thus about the same as before. From Set 3, taken after internal photoinjection, the interface-state density is 3.06×10^{11} cm^{-2}, approximately a 20% increase.

Further evidence is provided by the results of the following experiment. One of the samples was high-field stressed, with field plate positive, at 7.2 MV/cm for 60 min at 90°K. It was then warmed up and allowed to sit at room temperature for 17 hours with the gate short circuited to the substrate. At the end of this period the high frequency C-V curve was taken, which is Curve 1a in Fig. 3.4. The sample was then cooled to 90°K and the deep-depletion and light-assisted curves were taken. These are Curves 1b and 1c of Fig. 3.4. The sample was now subjected to internal photoinjection, using a photon energy of 5 eV. The injection field was first set at 1 MV/cm with the substrate negative. After the C-V curves had shifted to an almost saturated position, the injection field was reduced to 0.25 MV/cm. When the C-V curves had again shifted to an almost saturated position, the internal photoinjection was terminated. Curves 2b and 2c are the 90°K C-V curves taken after the internal photoinjection. The sample was then warmed to 66°C, and the high frequency C-V curves were taken. This is Curve 2a of Fig. 3.4. The horizontal distance between the parallel portions of Curves 2b and 2c (width of ledge) is greater than the corresponding distance between Curves 1b and 1c, indicating again an increased number of interface states after internal photoinjection.

3.3(C). Discussion

When one attempts to measure the electron capture cross section of the electron traps by monitoring the C-V shift as a function of the total amount of photoinjected electrons, one finds the accompanying generation of interface states to be a very undesirable feature. Fortunately, by examining the relations between the solid and the dashed curves in Fig. 3.4, we are still able to find the C-V shift that is due only to the oxide charge. In Fig. 3.4, Curve 2a is almost exactly parallel to Curve 1a. The near parallelism indicates that the shift ΔV_a between Curve 1a and Curve 2a is due mainly to the increase in the oxide charge. If ΔV_a is compared with ΔV_b, we find that these two quantities are very nearly the same. This relationship was found also to hold with other samples which were subjected to similar treatment. From Eq. (2.1) we know that the shift ΔV_b is due to

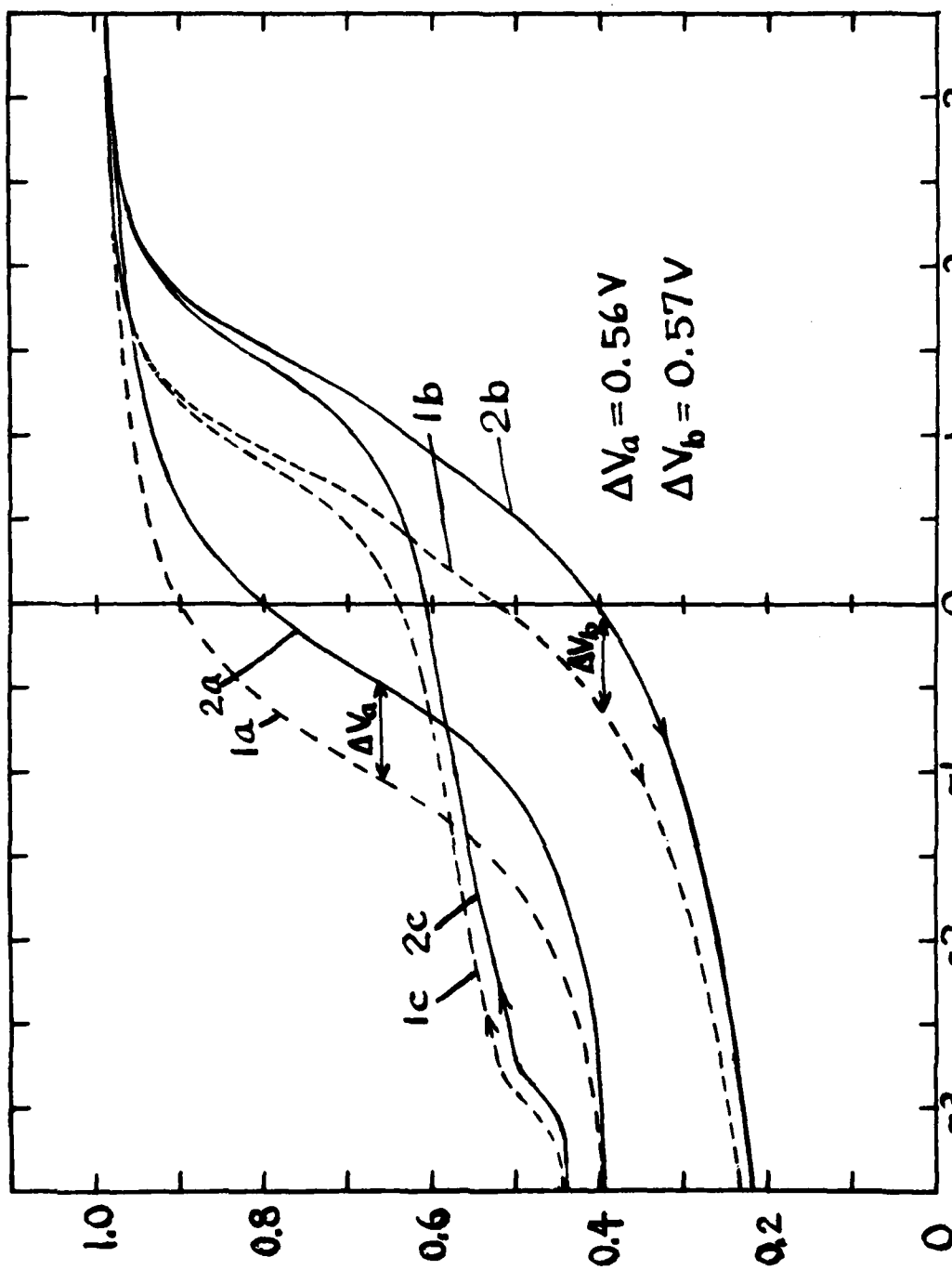

Fig. 3.4. Sample was first high-field stressed at 7.3 MV/cm for 60 min at 90°K. Curve 1a: After warming to 66°C. Curves 1b and 1c: Deep-depletion and light-assisted curves at 90°K. Curves 2b and 2c: After cooling to 90°K and internal photoinjection of electrons. Curve 2a: After warmup to 66°C.

an increase in either the equivalent oxide charge (Q_{ox}) or the interface states (N_{sa}, N_{sav}, or N_{sdc}). Now since ΔV_a is due mostly to the increase in the oxide charge, and $\Delta V_a \simeq \Delta V_b$, we may conclude that ΔV_b is also due mainly to the increase in the oxide charges.

The physical mechanism which is responsible for the aforementioned interface-state generation is still under investigation.

3.4. Some Properties of Electron Traps Generated in SiO_2 by High-Field Stress

3.4(A). Introduction

We have reported previously on our observations that electron traps are generated in silicon dioxide by high-field stress ($E \gtrsim 7$ MV/cm). The traps are deep, the optical depth being over 4 eV; thus they are different in character from the 2.4-eV electron traps which were studied by DiMara, Feigl, and Butler[60] and which have been tentatively attributed to sodium incorporated into the SiO_2 during growth.[61] Furthermore the traps, before the capture of electrons, do not produce an observable positive charging of the oxide, and so they appear also to be different from the positive electron trapping centers, studied by Ning and Yu,[55] Ning, Osburn, and Yu,[62] and Ning,[63] which have been observed in fresh SiO_2 samples and which can be diminished in number by an anneal in forming gas. By the same token, they appear to be different from the radiation-induced positive electron trapping centers studied by Aitken and Young[64] and by Aitken, DiMaria, and Young.[65] In a recent paper, Harari[66] has reported on a high-field generation of electron traps, perhaps similar to ours, in ultrathin (30-300 Å) films of silicon dioxide, and he suggests that the high-field breakdown of these thin films may be initiated by the generation and charging of these traps. One may speculate on whether the high-field generation of electron traps may be a contributing factor in the electron trapping in IGFET insulators that results in a threshold instability as reported by Ning, Osburn, and Yu.[67,68] Short-channel IGFETS operating with high electric fields should be particularly susceptible to this difficulty. In the present chapter we give some recent results on the measurement of electron capture cross sections of high-field-generated electron traps, and we show some preliminary results on the trap generation rates.

3.4(B). Samples and Experiment

The samples used in these experiments were RCA HCl-steam grown SiO_2 films with a thickness of about 1950 Å. The substrates were n-type (100) silicon having 5-10 Ω-cm resistivity. The front contacts of the capacitors were semi-transparent Al gates.

Because of the extremely long miniority-carrier response time[21] in the Si substrate for these samples, the quasi-static and high-frequency C-V curves were taken when the sample was warmed up to a temperature of 65-67°C. This allows a faster ramping rate to be used in taking the quasi-static C-V curves. Also, the noise-induced errors were greatly reduced.

The experimental procedure was as follows. The initial quasi-static and high-frequency C-V curves of a fresh sample were first taken at 66°C. The sample was then cooled to 90°K and the deep-depletion and light-assisted curves were taken. High-field stress with field plate positive was then applied to the sample. After this treatment, another set of low-temperature C-V curves were taken. The sample was warmed up to 66°C where a set of C-V curves (both quasi-static and high frequency) were taken. The sample was immediately cooled down to 90°K and the C-V curves were measured. The sample was then warmed up and allowed to set at room temperature until the interface state density increased to its saturation value (see the next section). The sample was then cooled to 90°K again. Electrons were internally photoinjected using 5 eV photons and an oxide field of approximately 1 MV/cm (with substrate negative). The shift of the deep-depletion curve was monitored to obtain a measure of the oxide charge. After the deep-depletion curve had shifted to an almost saturation position, the internal photoinjection was continued with a reduced oxide field of about 0.25 MV/cm until the final saturation of the shift was accomplished. (The reduced field was used at the end because of the possibility that the capture cross section may be reduced at high fields). After the internal photoinjection process, the sample was warmed up. Another set of 66°C and 90°K C-V curves were then taken.

3.4(C). Theory for Obtaining Capture Cross Section

By assuming that only a single species of trap is present in the oxide, and assuming that no detrapping is occurring during the photoinjection procedure, the following equation can be written to describe the trapping process:[53]

$$\frac{dn_t}{dt} = \sigma v_n n(N_t - n_t) \tag{3.6}$$

where σ is the capture cross section of the traps, v_n is the velocity of the free electrons, n is the density of the free electrons, n_t is the density of the trapped electrons, and N_t is the density of traps.

If only a small portion of the injected electrons are trapped, the injection current, j, is related to n as follows:

$$j = q v_d n \tag{3.7}$$

where v_d is the drift velocity of the electrons. With a field of 1 MV/cm at 90°K, v_d can be expected to reach a saturation value which is somewhat larger than the thermal velocity of the electrons at 90°K,[54] and, to a good approximation, we can use v_d in Eq. (3.6). Then, from Eqs. (3.6) and (3.7) we have

$$\frac{dn_t}{dt} = \sigma j (N_t - n_t)/q \tag{3.8}$$

The solution to this equation is

$$n_t(t) = N_t [1 - \exp(-\sigma N_{inj})] \tag{3.9}$$

where

$$N_{inj} = q^{-1} \int_0^t j \, d t$$

If we assume that the centroid of $n_t(t)$ remains the same as N_t, then Eq. (3.9) is equivalent to

$$\Delta V(t) = \Delta V_{sat}[1 - \exp(-\sigma N_{inj})] \tag{3.10}$$

where $\Delta V(t)$ is the C-V shift due to the presence of the trapped charges $n_t(t)$ in the oxide, and ΔV_{sat} is the shift when all the traps N_t are filled.

From Eq. (3.10) we have

$$\ln (1 - \Delta V(t)/\Delta V_{sat}) = -\sigma N_{inj} \tag{3.11}$$

3.4(D). Results

Figure 3.5 shows a plot of $\ln(1 - \Delta V(t)/\Delta V_{sat})$ against N_{inj} for three samples. Each had been high-field stressed for 30 min at fields of 7.2, 7.3, and 7.4 MV/cm respectively. The three sets of data agree well with each other and plot reasonably well on a straight line. The capture cross section determined from these data by use of Eq. (3.11) is $\sigma = 8.4 \times 10^{-14}$ cm^2.

In Fig. 3.6 we show a similar plot for three samples which were all high-field stressed at 7.2 MV/cm for periods of 10 min, 20 min, and 60 min respectively. The data here show somewhat greater differences than those of Fig. 3.5 and indicate capture cross sections that range from 8.4×10^{-14} to 9.5×10^{-14} cm^2, with the larger cross sections consistently corresponding to smaller stress times.

The values of ΔV_{sat} obtained at E = 7.2 MV/cm were used to calculate the corresponding values of electron trap density, N_t cm^{-2}, for various times of stressing. The results, which are plotted in Fig. 3.7, suggest that the generation of traps tends to saturate as the time of stress increases. The effect of the magnitude of the field at constant stress time is being investigated.

3.4(E). Discussion

(a) Comments on the Method of Obtaining Capture Cross Section

In using Eq. (3.11) we assume that the measured saturation voltage shift of the deep-depletion curve is the true saturation shift which corresponds to complete trap filling. In fact, the measured ΔV_{sat} can be expected to be at least slightly less than the true ΔV_{sat}. The result of this error, as can be analyzed from Eq. (3.11), is to make the $\ln(1 - \Delta V_t(t)/\Delta V_{sat,measured})$ vs N_{inj} plot curve up relative to the ideal straight line. The discrepancy between the two curves is given in dimensionless form by:

$$\Delta = \frac{\Delta(\Delta V_{sat})\ \Delta V(t)}{(\Delta V_{sat})^2\ (1 - \Delta V(t)/\Delta V_{sat})}$$

where ΔV_{sat} is the true saturation voltage, $\Delta(\Delta V_{sat})$ is the difference between the true and the measured saturation voltages. The discrepancy is smaller when $\Delta V(t)/\Delta V_{sat}$ is smaller. With a fixed $\Delta(\Delta V_{sat})/\Delta V_{sat}$, the initial portion of the measured curve will always give a better reading of

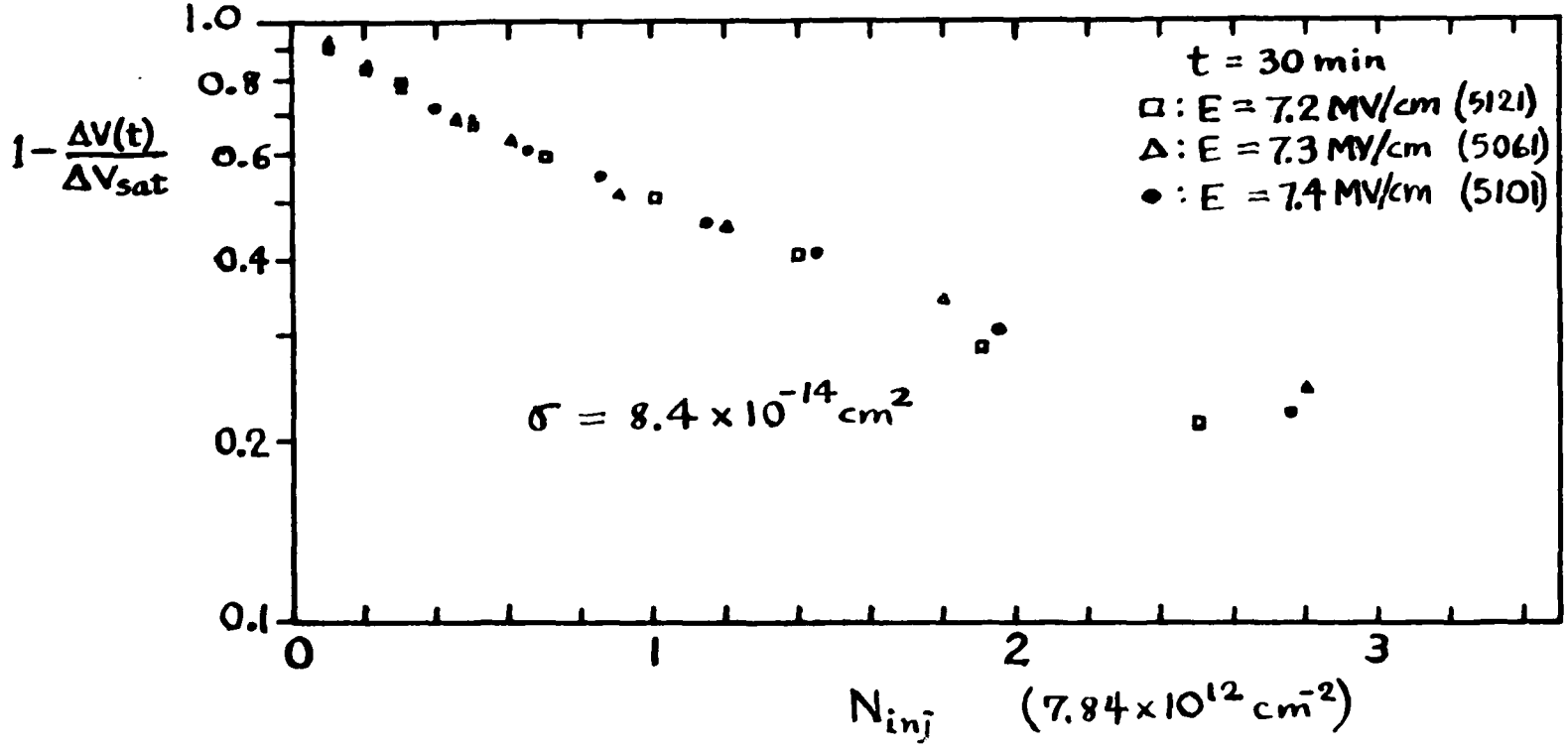

Fig. 3.5. Log plot of $(1 - \Delta V(t)/\Delta V_{sat})$ vs. N_{inj} for samples subjected to high-field stress for 30 min at fields of 7.2 MV/cm, 7.3 MV/cm, and 7.4 MV/cm respectively.

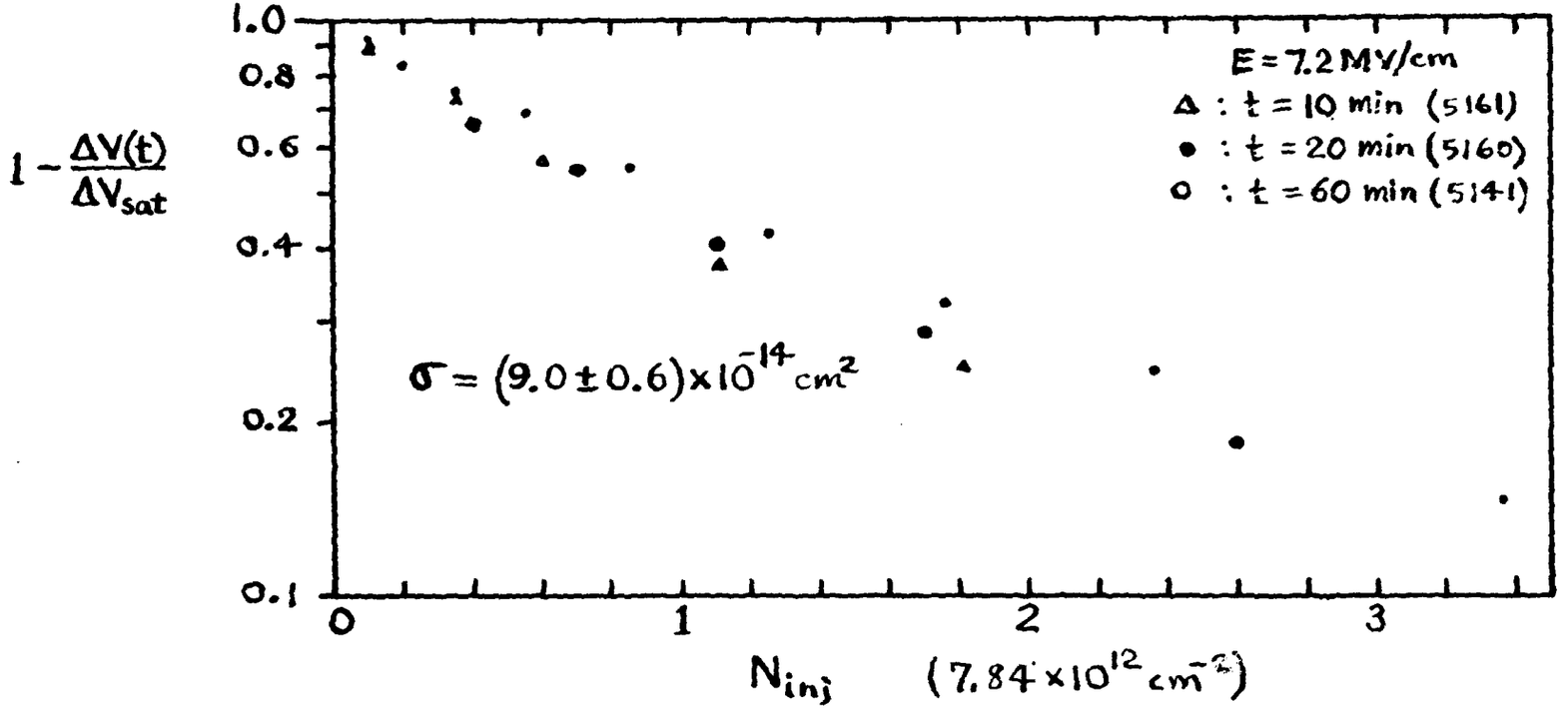

Fig. 3.6. Log plot of $(1 - \Delta V(t)/\Delta V_{sat})$ vs. N_{inj} for samples subjected to a fixed field stress of 7.2 MV/cm for periods of 10, 20 and 60 min respectively.

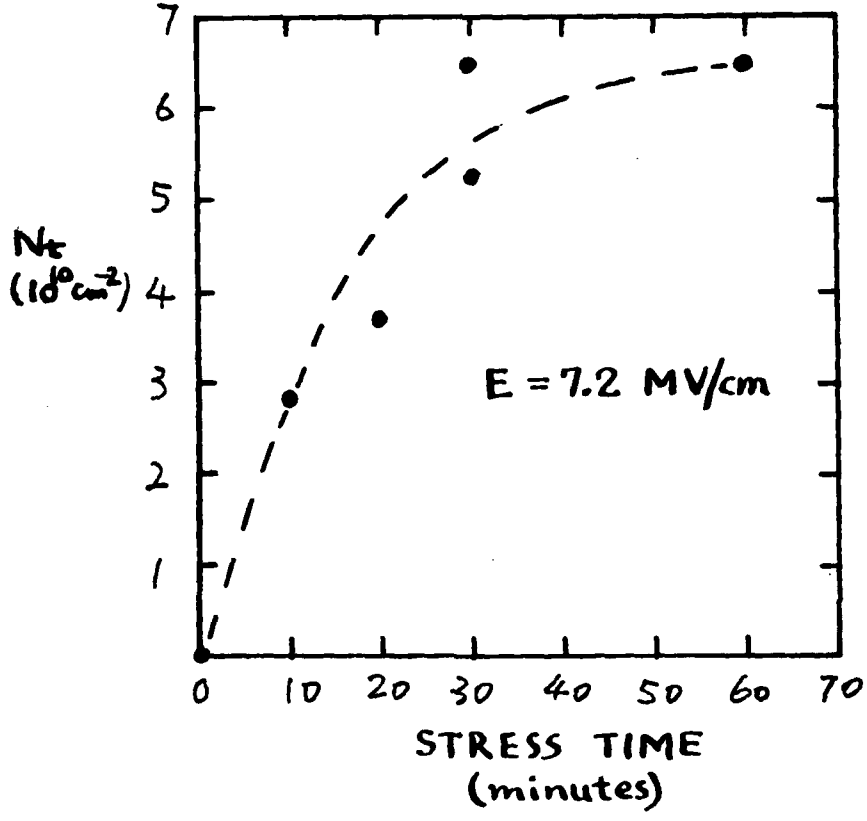

Fig. 3.7. Number of electron traps generated by high-field stress as a function of stress time. The stress field was 7.2 MV/cm.

the capture cross section.

Another possible reason for nonlinearity of the measured curve may be the existence of two or more species of traps with different capture cross sections. If there are two non-interacting species of traps with capture cross section σ_1 and σ_2, then we have the following equation.

$$1 - \frac{\Delta V(t)}{\Delta V_{sat}} = r_1 \exp(-\sigma_1 N_{inj}) + r_2 \exp(-\sigma_2 N_{inj})$$

where $r_1 = N_{t1}/(N_{t1} + N_{t2})$, $r_2 = N_{t2}/N_{t1} + N_{t2}$. Here N_{t1} and N_{t2} are the total trap densities of Species 1 and 2, respectively. This equation shows clearly that the effect of the second species of trap is to curve the $\ln(1 - \Delta V(t)/\Delta V_{sat})$ vs N_{inj} plot upward. If σ_1 is greater than σ_2 by, say, an order of magnitude, then the effect of the second term will remain small as long as N_{inj} is not large. Here we again find that the initial portion of the measured curve provides a better reading for capture cross section. If we are to find the values of both σ_1 and σ_2, we have to be able to increase N_{inj} by at least two more orders of magnitude, a procedure which may not be feasible because of limitations on intensity of the UV source.

Finally, instead of Eq. (3.11) there is an equivalent form[55] of Eq. (3.6) which avoids the requirement for determining ΔV_{sat}. However, this form requires the injection current to be constant, a requirement which is quite difficult to achieve with the present experimental setup.

(b) Comments on the Results

As was shown in Fig. 3.5, the capture cross section seems to be constant over the range of field strengths used there. However, Fig. 3.6 shows small but appreciable differences in cross section for different stress times. More experimental data are required to determine whether this is due to experimental error or is a true effect.

A value of 8.4×10^{-14} cm^2 for a capture cross section might be taken to indicate that the capturing center is coulomb-attractive and therefore positive in polarity before capture of an electron. No negative C-V shift corresponding to such a positive charge was found however, on a sample after it was high-field stressed at a field slightly below 7.3 MV/cm.

One way to explain the apparent coulumbic nature of the trapping center would be to postulate the existence of compensating pairs of charges with opposite signs. If this is true, the negative member of the pair might possibly serve as a hole trap.

3.4(F). Summary

The capture cross section of the electron traps generated by high-field stress at 90°K was found to be between 8.4×10^{-14} cm^2 and 9.5×10^{-14} cm^2. The density of the generated traps tends to saturate as the stress time increases. At 7.2 MV/cm, the density of electron traps appeared to saturate at about 7×10^{10} cm^{-2} at stress times of the order of 50 min.

3.5. Generation of Interface States After High-Field Stress at 90°K

3.5(A). Introduction

Various investigators have reported the generation of interface states in MOS capacitors after high-field stress at room temperature[21,80,81] and after negative-bias stress in the temperature ranges of 25°C - 125°C[56] and 250° - 450°C.[57,58] We have reported previously[25] that if the high-field stressing was performed at low temperature (91°K), the generation of interface states was not observed immediately, but instead the interface states made their appearance only after the sample was warmed. A further study of this subject is described in the following sections of this report.

3.5(B). Samples and Experiments

Three types of samples were used in this study. All had (100) n-type substrates. Samples RCA-1 and RCA-2 had HCl-steam grown oxides with thicknesses of approximately 2500 Å and 1950 Å, respectively, on silicon substrates having respective resistivities of 1-2 Ω-cm and 5-10 Ω-cm. The third type, Sample BTL, had a 3% HCl dry-grown oxide with a thickness of about 920 Å on a silicon substrate with a nominal resistivity of 5 Ω-cm. The Al gate for RCA-1 was about 1000 Å thick, and the samples designated RCA-2 and BTL had semitransparent Al gates.

The experimental procedures were as follows. A set of room-temperature (for RCA-1) or 66°C (for RCA-2 and BTL) C-V curves (quasi-

static and high frequency) were taken on the fresh sample, and the sample was then cooled to 90 ± 1°K. The low temperature C-V curves (deep-depletion and light-assisted) were taken, after which the sample was high-field stressed at a chosen field for a certain period of time. Following the high-field stress, a set of low-temperature C-V curves were recorded. The sample was then warmed up to room temperature (RCA-1) or 66°C (RCA-2 and BTL), and a set of room-temperature or 66°C C-V curves was taken. The sample was immediately cooled down to 90°K to take the corresponding low-temperature C-V curves. After this process the sample was warmed and allowed to sit at room temperature. A set of room-temperature (or 66°C) and low-temperature C-V curves were taken after certain periods of time.

In some cases, internal photoinjection of electrons was performed at 90°K immediately after the high-field stress treatment and before the first warm-up.

3.5(C). Results

Table I shows the interface-state densities (as obtained by the LTL method) of an RCA-1 sample before and after high-field stress at 91°K with a field of 7.6 MV/cm for 22 min. N_{ss} was found to be unchanged after the high-field stress if the sample was kept at 91°K. As the sample was warmed toward room temperature, N_{ss} increased rapidly. When the sample was held at room temperature, N_{ss} increased logarithmically with time. This is plotted in Fig. 3.8.

Two RCA-2 samples were high-field stressed at 90°K with the same field of 7.3 MV/cm for 30 min. Table II shows the history of N_{ss} for both samples. Sample 4201 was warmed up to room temperature and kept at this temperature for about 33 hrs with the gate short circuited to the substrate. Sample 4201 was warmed up and held at 55°C for 4 hrs with the gate short circuited(interface field nearly zero). Gate voltage was then applied so that the SiO_2-Si interface field was about 1 MV/cm for an additional 3 hrs. Again, N_{ss} remained unchanged at 90°K after the high-field stress. N_{ss} increased by approximately 37% over the initial N_{ss} for both samples when they were first warmed to 66°C for about 20 min (to take the 66°C C-V curves). If the interface field was kept at approximately zero, N_{ss} increased at a rate slower than the case of Table I regardless of whether the sample was at

Sample condition	N_{ss} (cm^{-2})	ΔN_{ss} (cm^{-2})
Initial	0.27×10^{11}	
		0
After high field stress		
Before warm up ..	0.27×10^{11}	
		1.57×10^{11}
1 hr in room T ..	1.84×10^{11}	
		0.41×10^{11}
11 hrs in room T ..	2.25×10^{11}	
		0.09×10^{11}
33 hrs in room T ..	2.34×10^{11}	
		0.11×10^{11}
105 hrs in room T ..	2.45×10^{11}	

Table I. N_{ss} obtained by the LTL method for stress and after high-field stress at 90°K with 7.6 MV/cm for 22 min followed by warm-up to room temperature. Sample RCA-1.

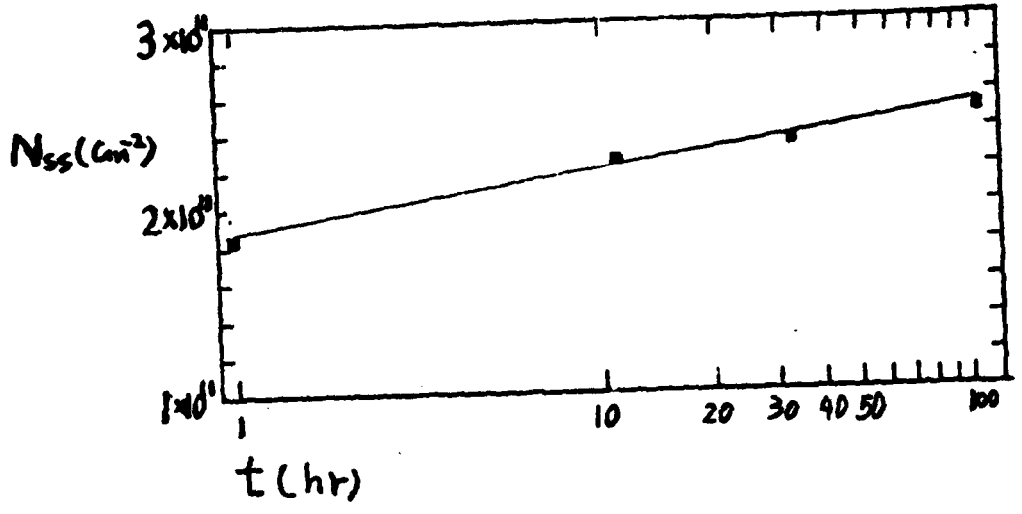

Fig. 3.8. Increase of interface states as a function of time after the sample was high-field stressed, warmed, and held at room temperature.

Sample No. 4200			Sample No. 4201		
	$N_{ss}(cm^{-2})$	$\Delta N_{ss}(cm^{-2})$		$N_{ss}(cm^{-2})$	$\Delta N_{ss}(cm^{-2})$
Initial	2.42×10^{11}	0.91×10^{11}	Initial	2.32×10^{11}	0.86×10^{11}
20 min at 66°C	3.33×10^{11}	0.09×10^{11}	20 min at 66°C	3.18×10^{11}	0.05×10^{11}
33 hr at 25°C $E_{SiO_2-Si} \doteq 0$ V/cm	3.42×10^{11}		4 hr at 55°C $E_{SiO_2-Si} \doteq 0$ V/cm	3.23×10^{11}	0.22×10^{11}
			3 hr at 55°C $E_{SiO_2-Si} \doteq 1$ MV/cm	3.45×10^{11}	

Table II. N_{ss} obtained by the LTL method for two RCA-2 samples subjected to the same high field stress (6.3 MV/cm for 30 min) but with different warm-up conditions.

25°C or 55°C. This difference between the generation rates may be due to the difference between the stress fields (7.6 MV/cm for Table I, 7.3 MV/cm for Table II). If an interface field of 1 MV/cm is applied (Sample 4201), the increase of N_{ss} is accelerated.

Table III shows the results obtained on a BTL dry-oxide sample which was high-field stressed at 90°K with a field of 7.4 MV/cm for 30 min. Observation of the interface states by the LTL method showed no generation of interface states at 90°K. The generation of states after warm-up is shown in Table III. The distribution of states within the silicon bandgap, n_{ss} in cm^{-2} eV^{-1}, is shown in Fig. 3.9 as calculated by Kuhn's method[42] before stress, after warm-up to 65°C for 20 min, and after 14 hrs at 25°C. A prominent feature in Fig. 3.9 is the peak in n_{ss} after the sample was first warmed up (Curve 2). This peak gradually reduced as the sample was held at room temperature. A similar peak in n_{ss} was observed by Roitman[28] in the interface states generated in the Si-SiO_2 system by electron-beam irradiation.

Figure 3.10 shows n_{ss} (cm^{-2} eV^{-1}) for the other BTL Sample. This sample was stressed at the same field and for the same time as the sample of Fig. 3.9, but internal photoinjection of electrons was performed before the same was warmed. This resulted in an appreciably reduced interface-state after warming. Also, the peak found in Fig. 3.9 is greatly reduced.

3.5(D). Discussion

The presence of holes[23,24,25] at the SiO_2-Si interface has been suspected to be a source of interface states.[31-33] We have found in this study, however, that even when the stress field is not high enough to cause impact ionization, so that after high-field stress only a net negative charge was detected in the oxide, interface states were still generated after the sample had been warmed up (Table II).

The general pattern for the generation of interface states after high-field stress at 90°K can be summarized as follows. First, no generation can be observed for several hours at 90°K after high-field stress. Secondly, the generation rate increases as the temperature is raised. For example, the generation of interface states was observed when one sample was warmed up to 168°K and then brought back immediately to 90°K (see also J. J. Clement's results in Ch. 2 of this report). Thirdly, at room temperature the interface-

Sample condition	N_{ss} (cm^{-2})	ΔN_{ss} (cm^{-2})
Initial	0.51×10^{11}	
After high field stress:		0
Before warm up..	0.51×10^{11}	2.11×10^{11}
20 min at 65°C..	2.62×10^{11}	0.09×10^{11}
14 hr at 25°C..	2.71×10^{11}	

Table III. N_{ss} obtained by the LTL method for a BTL sample which was high-field stressed at 7.4 MV/cm for 30 min and warmed.

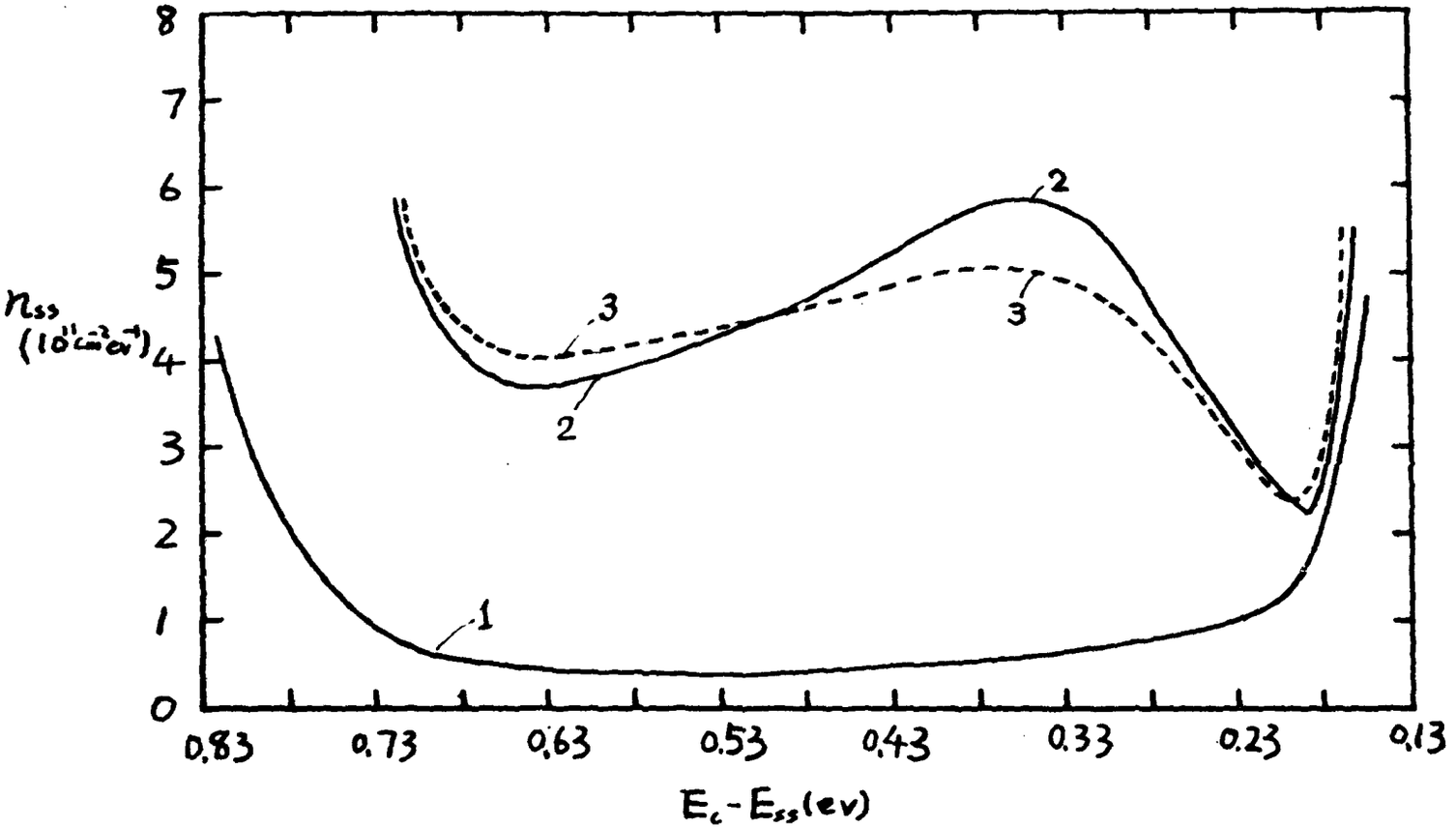

Fig. 3.9. Plots of n_{ss} (cm^{-2} eV^{-1}) as a function of the energy below the Si conduction band edge for a BTL sample before the high-field stress (Curve 1), after stress at 90°K with 7.4 MV/cm for 30 min followed by warming to 66°C (Curve 2), and after the sample had been at room temperature for 14 hours (Curve 3).

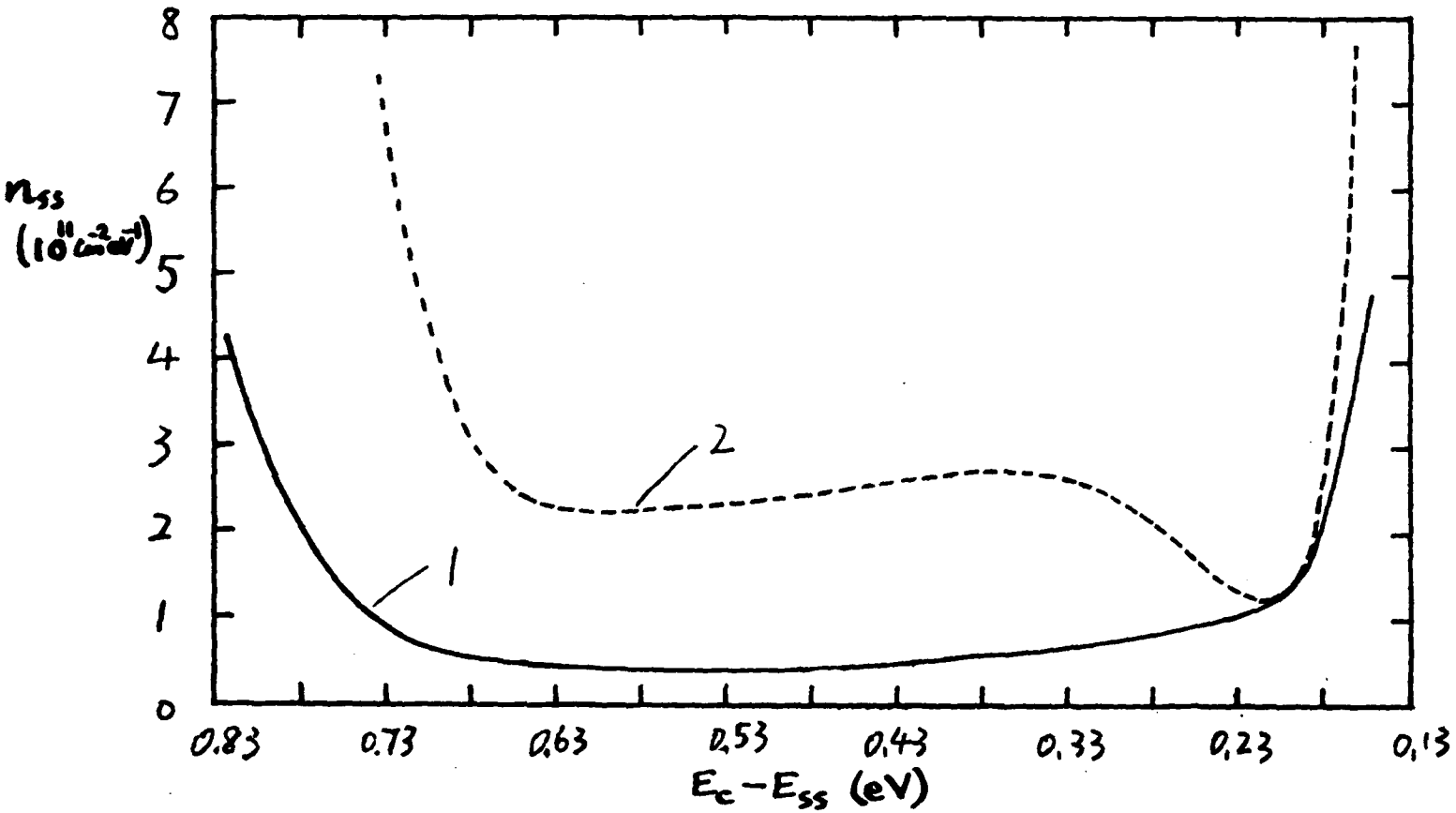

Fig. 3.10. Plots of n_{ss} (cm^{-2} eV^{-1}) as a function of the energy below the Si conduction-band edge for a BTL sample before it was field stressed (Curve 1), after high-field stress followed by internal photoinjection, and warming to 66°C (Curve 2).

state density continues to increase slowly and follows approximately a linear function of ln t, as shown in Fig. 3.8. The generation rate can be accelerated by the assistance of a moderate field, as in Sample 4201 of Table II.

The peak of n_{ss} in Fig. 3.9 suggests the possibility of a bond-breaking process during the high-field stress. The height of the peak is reduced while the width is increased as time goes on. This may indicate that a process of atomic rearrangement is taking place at the SiO_2-Si interface. Thermal energy may be required for the rearrangement.

From a comparison of Figs. 3.9 and 3.10 it would appear that the injection of electrons through the SiO_2-Si interface can anneal out a considerable portion of the potential defects which, when supplied with sufficient thermal energy, give rise to interface states. This further recommends the possibility of the aforementioned bond-breaking process. When electrons are injected through the interface, some of the broken bonds may become satisfied by capture of free electrons. Further study of the interface-generation phenomenon is indicated.

4. INVESTIGATION OF HIGH-FIELD EFFECTS IN Al-Al_2O_3-Si CAPACITORS
(O. Bar-Gadda collaborating)

We report here on the continuation of experiments relating to charge storage and dielectric breakdown in Al_2O_3 on silicon substrates.

4.1. Samples

The samples used in this study were fabricated at Bell Laboratories, and we thank G. E. Smith, D. M. Boulin, and E. Labate for their aid. The substrates of the samples were (100) 4-6 ohm-cm silicon. Both n (P-doped) and p (B-doped) substrates were included. CVD Al_2O_3 films were deposited to thicknesses of 450-480 Å, using two deposition temperatures: 815°C and 900°C. The samples had Al field plates approximately 1000 Å in thickness.

As received, the MIS capacitors showed intial flatband voltages in the range 1.0 ± 0.3 V, corresponding to an average fixed oxide charge of $\sim 2 \times 10^9$ cm^{-2}.

4.2. Experimental Procedures

The following experiments were performed on these samples:

(1) The flatband voltage, V_{FB}, vs. time t was measured for different applied fields, E_a for both field polarities and substrate types.

(2) The time to breakdown, t_B, vs. applied field, E_a, was measured for substrate biased in accumulation.

(3) C-V curves were recorded before and after breakdown.

(4) Oscillograms of the breakdowns were recorded.

(5) Samples were observed under an optical microscope after breakdown.

All experiments were carried out at room temperature. The voltages were applied by either of two pulse generators. The first, used in the pulse-width range $\Delta\tau > 10$ ms had a rise time of ~ 10 μs. The second, used in the range $\Delta\tau < 10$ ms, had a rise time of ~ 30 ns.

4.3. Results and Discussion

Figure 4.1 shows the results of Procedure (1), as described above, for samples biased in accumulation. In general, for the p-type samples, ΔV_{FB} tended to saturate at ~ 4 V, then decreased, the decrease being accompanied

by a large stretchout of the C-V curve. For the n-type samples, however, no saturation is apparent. The maximum flatband shift for positive bias on n-type is $\sim$ 7 V.

For negative bias on n-type and positive bias on p-type, an incandescent light was used to illuminate the samples so as to maintain the inversion layer. Deep depletion would be an undesirable condition for studying the oxide, for two reasons: (a) Part of the applied field would appear across the depletion layer, and (b) impact ionization of carriers in the depletion layer would create hot carriers.

The results for illuminated samples biased in inversion were very similar to those shown in Fig. 4.1. Qualitatively, we can say that (i) the charging is faster in the n-type sample than in the p-type sample for a given field and polarity, (ii) the maximum ΔV_{FB} for positive bias is greater for p-type than for n-type, (iii) saturation appeared to occur in all cases except for positive biased n-type at the higher bias voltages. In the case of negative bias, saturation was accompanied by large C-V stretchout followed by a decrease in ΔV_{FB}.

The injection mechanism cannot be inferred from the ΔV_{FB} vs. t curve because nearly all types of injection will produce similar curves. For Al_2O_3, it is believed that direct tunneling of electrons to traps plays an important role because of the relatively low field (1-2 MV/cm) required for measurable injection current and charge trapping and because the measured density of electron traps ($\sim 10^{18} - 10^{19}$ cm^{-3}) is high. We did not study the injection mechanism. It is unlikely that ionic current plays a role here because the flatband shift is positive for all polarities of applied field.

A possible model for the charging process is illustrated in Fig. 4.2. The field initially injects electrons from the Al into the oxide (Sketch a) where some of them are trapped (Sketch b). This reduces the injection field, decreasing the external current. The field near the positive contact increases, and this leads to a reduction in negative charge in the oxide (Sketch c) by a mechanism which is unclear at present. Electron emission from neutral centers or hole trapping near the Si interface are two possibilities. The sequence of events with positive gate bias is probably similar to the above, but the reduction in negative charge would

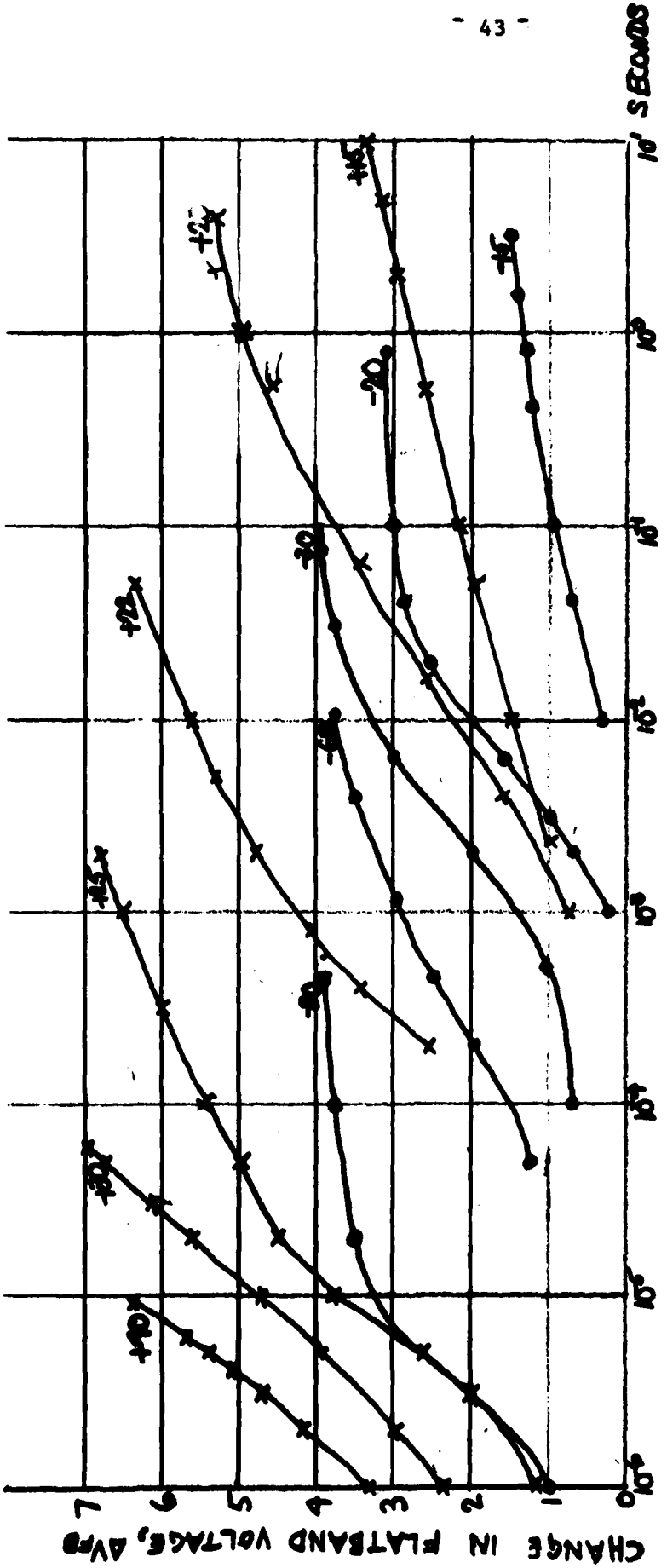

Fig. 4.1. ΔV_{FB} vs. $\log t$ for various gate voltages (as labeled).
x : n-type • : p-type

not be observable because it would take place near the field plate and consequently would not result in an appreciable C-V shift.

Figure 4.3 is a plot of time-to-breakdown vs. applied field for the case of accumulation. The results indicate a threshold field for breakdown of $\sim$ -4.9 MV/cm for p-type, and $\sim$ +4 MV/cm for n-type. These fields are lower than the "intrinsic" field strengths measured for Al_2O_3 (> 6 MV/cm), which suggests that the breakdowns are due to weak spots or, alternatively, that the maximum field in the oxide is significantly larger than the average field.

Figure 4.4 shows typical C-V curves before and after breakdown. For all cases except positive bias on n-type, a complete C-V curve from accumulation to inversion is traceable. For (+) on n-type, a nearly total breakdown is observed in which the oxide has been completely discharged. For the case of negative bias, there is not much change in the oxide charge or the C-V curve, and indeed the only electrical means of noting the breakdown is the orders-of-magnitude sudden increase in current. For the case of positive bias on illuminated p-type, two features are observed: (1) a small positive ΔV_{FB} and (2) an apparent increase in the capacitance in the weak accumulation regime.

We illustrate in Fig. 4.5(a) a typical voltage waveform taken of a breakdown on positively biased n-type. The breakdown discharge takes place with a time constant on the order of 1 μs and is seen to be followed by a series of propagating breakdowns. Observation of the sample under an optical microscope reveals the presence of the breakdown areas. Features very similar to those reported for self-healing or self-quenched breakdowns are noted, such as the presence of a circular hole where breakdown is presumed to have evaporated the metal field plate. In addition we note that the breakdown spot displays an irregular star-shaped pattern with rays extending from it, possibly being filamentary conduction paths or cracks on the field plate. A final important feature should be noted. In all cases of breakdown observed, the breakdown spots occurred very close to the edge of the field plate. This suggests that the field at the edges may be considerably higher than that in the rest of the oxide, and quite conceivably close to the intrinsic field strength. An edge effect would seem to be an important

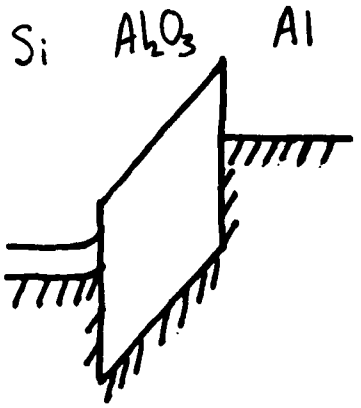

(a) Initial band configuration on application of bias.

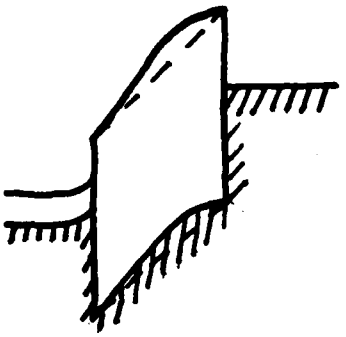

(b) After charging by electron trapping near Al and into the bulk.

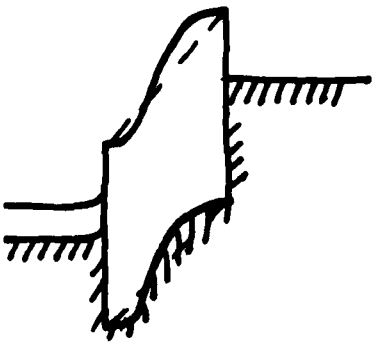

(c) After reduction of flatband shift, possibly caused by electron emission from neutral centers in bulk, or hole trapping near the Si interface.

Fig. 4.2. Band diagram for negative bias

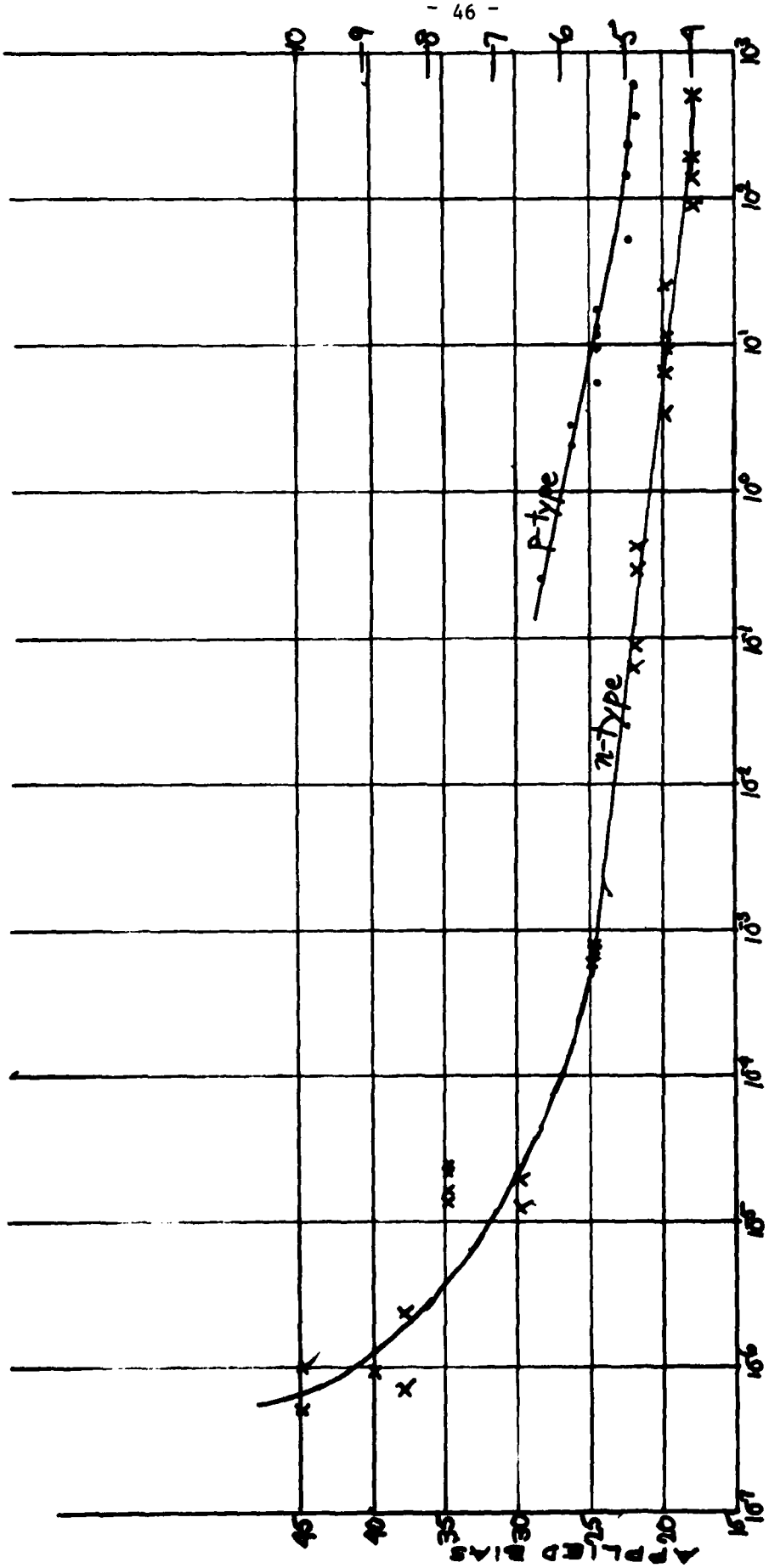

Fig. 4.3. Time to breakdown (s) vs. applied bias (VOLTS on left, MV/cm on right)
(Polarity: − for p-type; + for n-type)

Fig. 4.9 Typical C-V curves obtained before bias, after bias but before breakdown, and after breakdown.

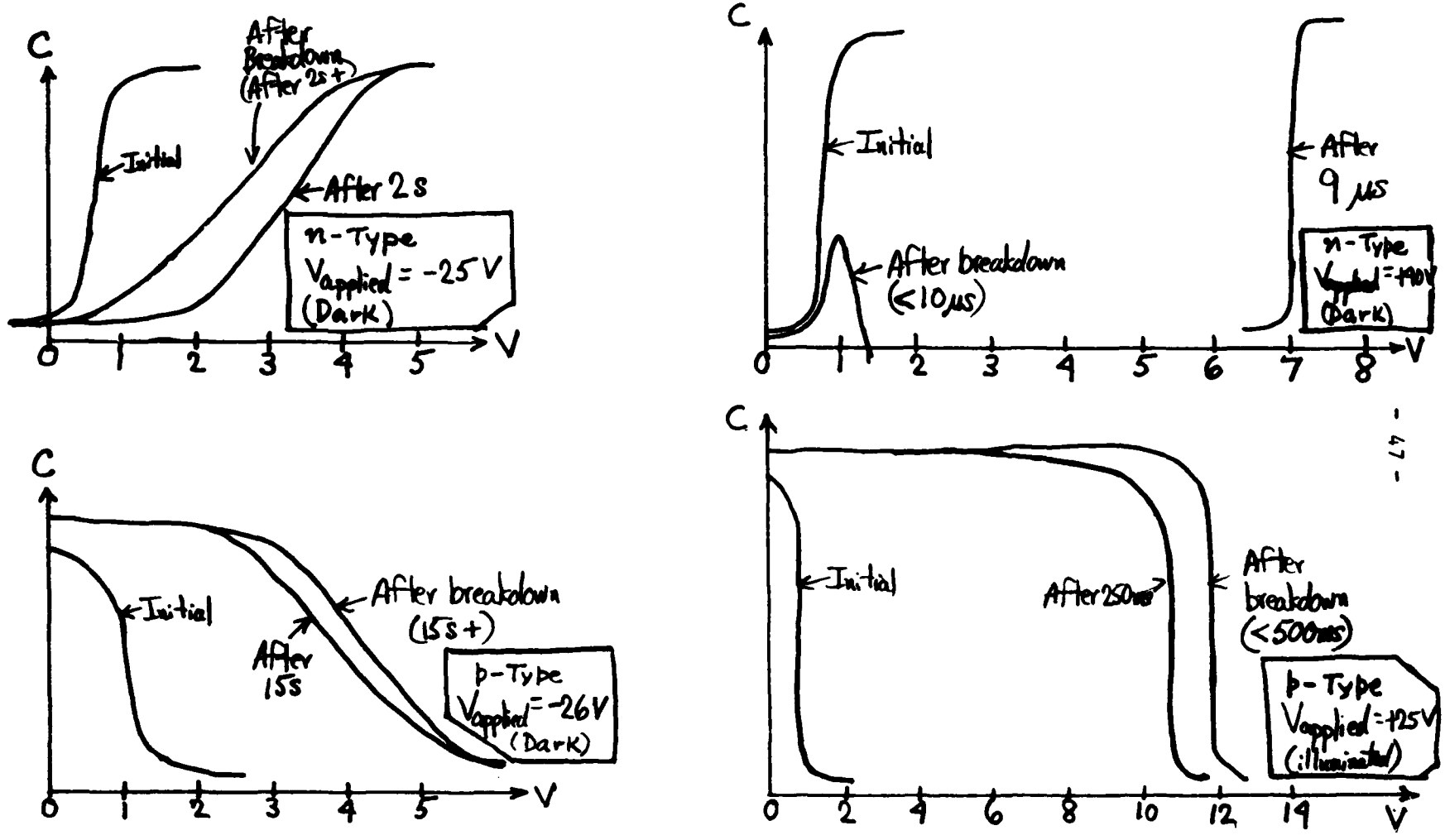

factor in the breakdown process. Finally, we note that high-field breakdown at the edges seems to imply the absence of pinholes or other severe weak spots in the film.

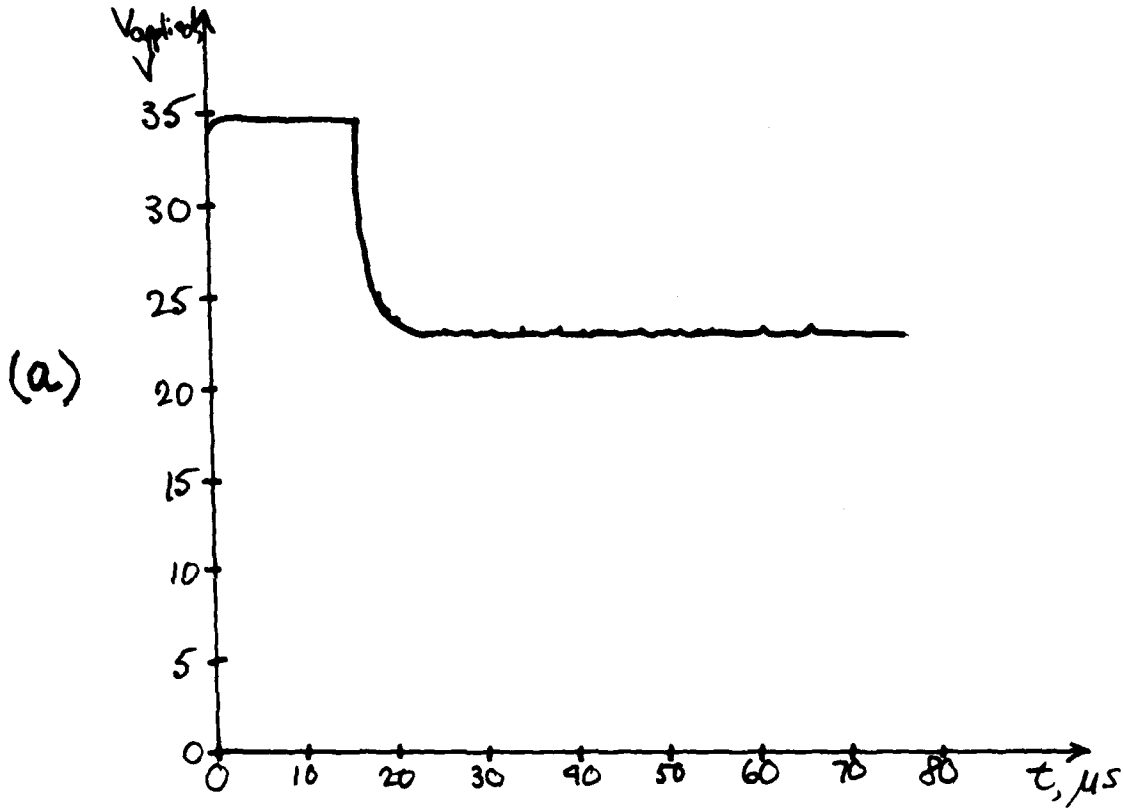

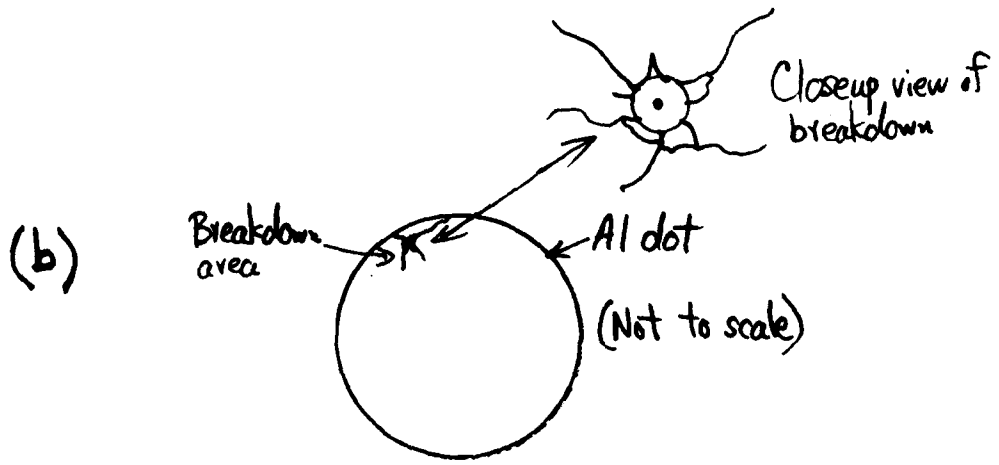

Fig. 4.5. Typical oscillogram and micrograph of breakdown

5. CORONA AND MIS STUDIES OF HIGH-FIELD EFFECTS IN Al_2O_3
(S. S. Li collaborating)

5.1. Introduction

Several investigators have observed that holes are generated and captured within the Al_2O_3 when the sample is exposed to X-rays[69] or VUV radiation.[70,71] Positive charging is also observed in Al_2O_3 after exposure to negative corona at high fields.[27] In this chapter we present experimental evidence which indicates that the positive charging observed in Al_2O_3 is due to the trapping of holes.

We have also investigated electron trapping in Al_2O_3. For this purpose we have utilized an internal photoemission of electrons into the Al_2O_3 under a low positive field. If we assume that the electron traps are uniformly distributed through the bulk of the oxide and that all have the same cross section, our results indicate a trap concentration of 1.9×10^{18} cm^{-3} and an electron trapping cross section of 3×10^{-13} cm^2.

5.2. Samples and Experimental Apparatus

The samples, which were fabricated at Bell Laboratories, had a 900°C pyrolytic Al_2O_3 film with a thickness of about 450Å. The substrate was n-type (100) silicon with 8-12 Ω-cm resistivity. The front Al gate of the MIS structure used in the photoinjection experiment was semi-transparent.

The set-up for the corona-charging experiment was described in Reference 23. The photoinjection experiments were performed with the sample mounted in a chamber which could be evacuated to a pressure of approximately 1 micron. The sample was exposed to UV light through a silica window. A Keithley 610B electrometer was used to monitor the external flow of charge. Charge storage in the insulator was determined from the flatband voltage of the MIS structure as measured at 1 MHz.

5.3. Constant-Current Negative Corona Charging

Negative corona was applied to charge the bare surface of the Al_2O_3 sample. The surface potential and flatband voltage as functions of the charging time are shown in Fig. 5.1 for three different current levels. Initially, the surface potential buildup and the flatband voltage decay are very fast. Negative flatband shift corresponds to the loss of

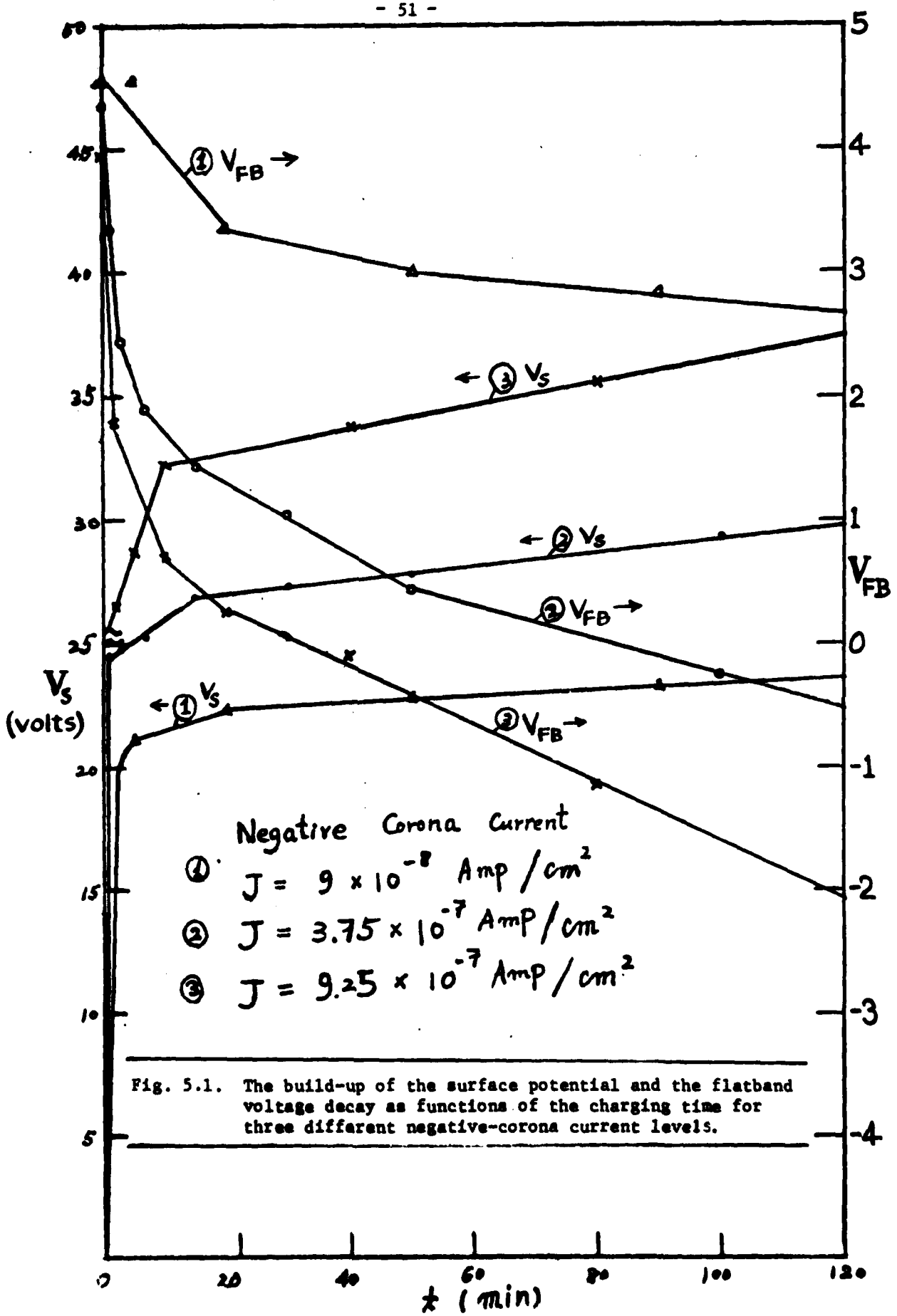

Fig. 5.1. The build-up of the surface potential and the flatband voltage decay as functions of the charging time for three different negative-corona current levels.

negative charge or the gain of positive charge. With high charging current and long charging times, the flatband voltage falls lower than -1 volt, indicating that a net positive charge exists within the oxide.

If the charged sample is exposed to low-level negative corona for a time, the C-V curve will shift to the right side. This indicates that part of the positive charge has been annealed out by the electrons injected from the front surface.

When a fresh sample is thermally annealed in vacuum at 500°C for one hour, no flatband shift is observed. This indicates that the negative charges within the fresh sample may be due either to deeply trapped electrons or to fixed negative charges. The positive charges found after negative corona treatment can be reduced appreciably if the surface charge is neutralized and the sample is annealed in vacuum at 300°C for 50 minutes. A 3 V positive flatband shift is observed with this treatment.

5.4. MIS Experiments

As is shown in Fig. 5.2, biasing the MIS capacitor to an average field of -4.7 MV/cm for 10 minutes causes a positive flatband shift and a large hysteresis that was not present in the C-V curves of the fresh sample. As the sample biasing time is increased, the C-V curves begin to shift to the left, indicating a loss of negative charge or a gain of positive charge. This agrees with an observation made by Tsujide.[72] The hysteresis can be attributed to the injection of electrons which neutralizes holes captured close to the interface. It appears that positive charge trapping exists only after negative biasing. There are several possibilities:[27]

(a) Holes may be injected from the substrate.

(b) Electrons may tunnel out of neutral centers and leave positive charge behind.

(c) Injected electrons from the front surface might obtain enough energy to impact-ionize the lattice or neutral traps. The generated holes may then be captured.

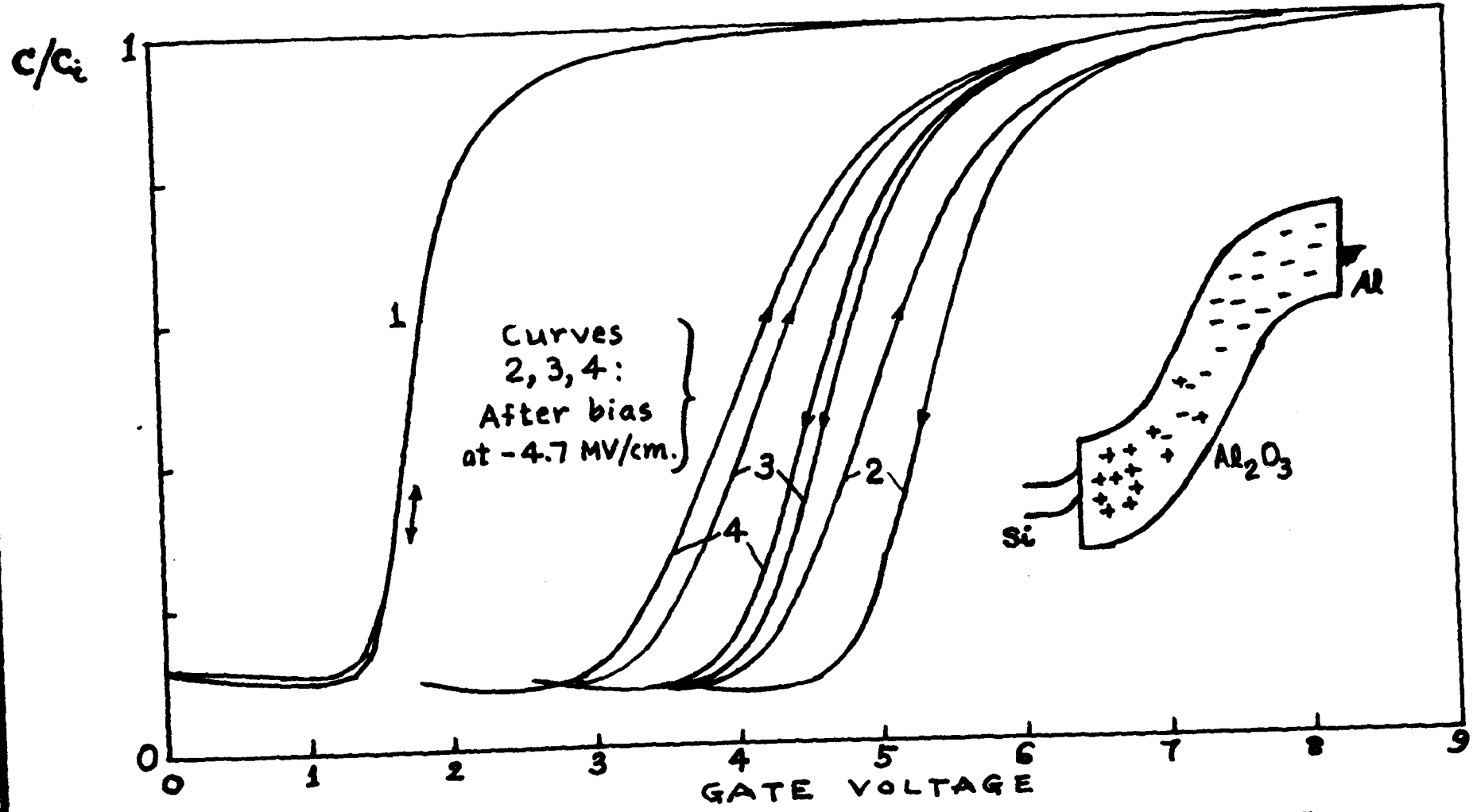

Fig. 5.2. C-V curves for the Al-Al_2O_3-Si capacitor. (1) Fresh sample. (2) After 10 min, -21 V. (3) After total of 30 min, -21 V. (4) After total of 60 min, -21 V. Also shown is a band diagram illustrating the charge storage.

Impact ionization will depend very much on the mean free path of the charge carriers in the oxide. The optical phonon scattering length is about 4-5 Å,[70,71,73] which is one-sixth of that in SiO_2,[74,75] and the optical phonon energy is about 0.1 eV. Taking this into account, we can see that the number of hot electrons will be quite limited. Also, it is probable that generated holes will suffer geminate recombination even in high fields.[71] Therefore, impact ionization appears to be an unlikely source of holes.

From the above argument, we propose the following charge-trapping model for the Al-Al_2O_3-Si structure under negative high-field stress. Electrons can tunnel from the Al gate and be captured in the bulk of the Al_2O_3. Holes are injected from the substrate and are trapped. The centroid of the trapped electrons is close to the front surface, but the centroid of the holes is near the Al_2O_3-Si interface (Fig. 5.2). The electron and hole trapping reduces the field at both interfaces, thus enhancing the field in the bulk. This explains why the current decays with time, and will also be a factor in the breakdown of the oxide.

5.5. Capture Cross Section and Concentration of Electron Traps

The Al-Al_2O_3-Si sample was held at a bias of 1.2 MV/cm until the dark current fell below 10^{-11} A/cm^2. Electrons were then photoinjected from the substrate into the Al_2O_3 by 5 eV UV light. The external current and the flatband shift were measured after each 30-sec interval of exposure.

It has been shown by Harari and Royce[69] and by N. Johnson,[76] using the results of photodepopulation experiments, that electron traps are distributed almost uniformly through the bulk of the oxide. Therefore in our analysis we assume that the traps are uniformly distributed and that all the traps have the same electron trapping cross section. Under the assumption that photodetrapping and field detrapping are small enough to be neglected, the equations which determine the trapped electron concentration, $n_T(x,t)$, are[77]

$$q \frac{\partial n_T(x,t)}{\partial t} = - \frac{\partial j(x,t)}{\partial x} \tag{5.1}$$

and

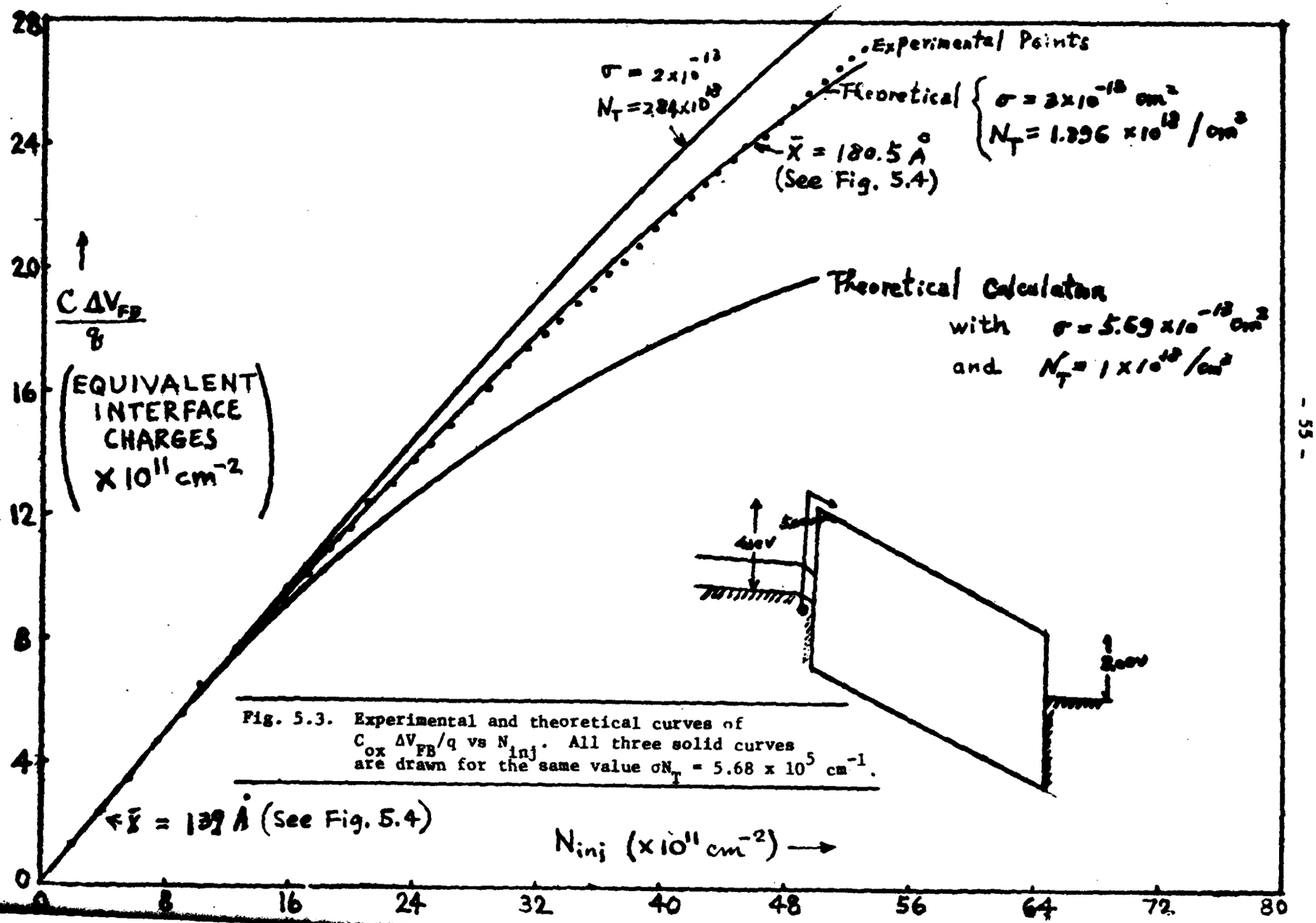

Fig. 5.3. Experimental and theoretical curves of $C_{ox} \Delta V_{FB}/q$ vs N_{inj}. All three solid curves are drawn for the same value $\sigma N_T = 5.68 \times 10^5$ cm^{-1}.

$$q \frac{\partial n_T(x,t)}{\partial t} = \sigma j(x,t) \; [N_T - n_T(x,t)] \tag{5.2}$$

where σ is the electron capture cross section. The solution is[77,78]

$$n_T(x,t) = N_T [\exp(\sigma N_{inj}) - 1]/[\exp(\sigma N_{inj}) - 1 + \exp(\sigma N_T x)] \tag{5.3}$$

where N_{inj} is the number of injected electrons per unit area and is given by

$$N_{inj} = C_{ox} \Delta V_{FB}/q + Q_{ext}/q \tag{5.4}$$

Here Q_{ext} is the amount of charge that flows through the external circuit during the photoinjection process.

The effective trapping efficiency is defined by

$$\eta_{eff} (N_{inj}) = \frac{d(C_{ox} \Delta V_{FB}/q)}{d N_{inj}} \tag{5.5}$$

Thus,

$$\eta_{eff}(0) = 1 - [1 - \exp(- \sigma N_T t_{ox})]/\sigma N_T t_{ox}. \tag{5.6}$$

From. Eq. (5.5) we see that the initial slope of $C_{ox} \Delta V_{FB}/q$ vs N_{inj} will give $\eta_{eff}(0)$, which can be used to determine $N_T\sigma$. In Fig. 5.3 we show the experimental data. These fit the theoretical calculation very well with the values $N_T = 1.9 \times 10^{18}$ cm^{-3} and $\sigma = 3 \times 10^{-13}$ cm^2. Our measured trap density is consistent with the number of negative trapped charges, $10^{17} - 10^{18}$ cm^{-3}, measured by Mehta, Butler, and Feigl[79] in their samples of Al_2O_3.

The centroid of the electron trapping vs N_{inj}, as calculated from n_T and ΔV_{FB}, is plotted in Fig. 5.4. The centroid advances from 139 Å to 181 Å gradually until the photoinjection is stopped. The initial electron trapping efficiency is computed to be 92.2%.

5.6. Discussion

Trapped holes are observed after the Al_2O_3 has been under negative high-field stress. The small electron-optical phonon scattering length

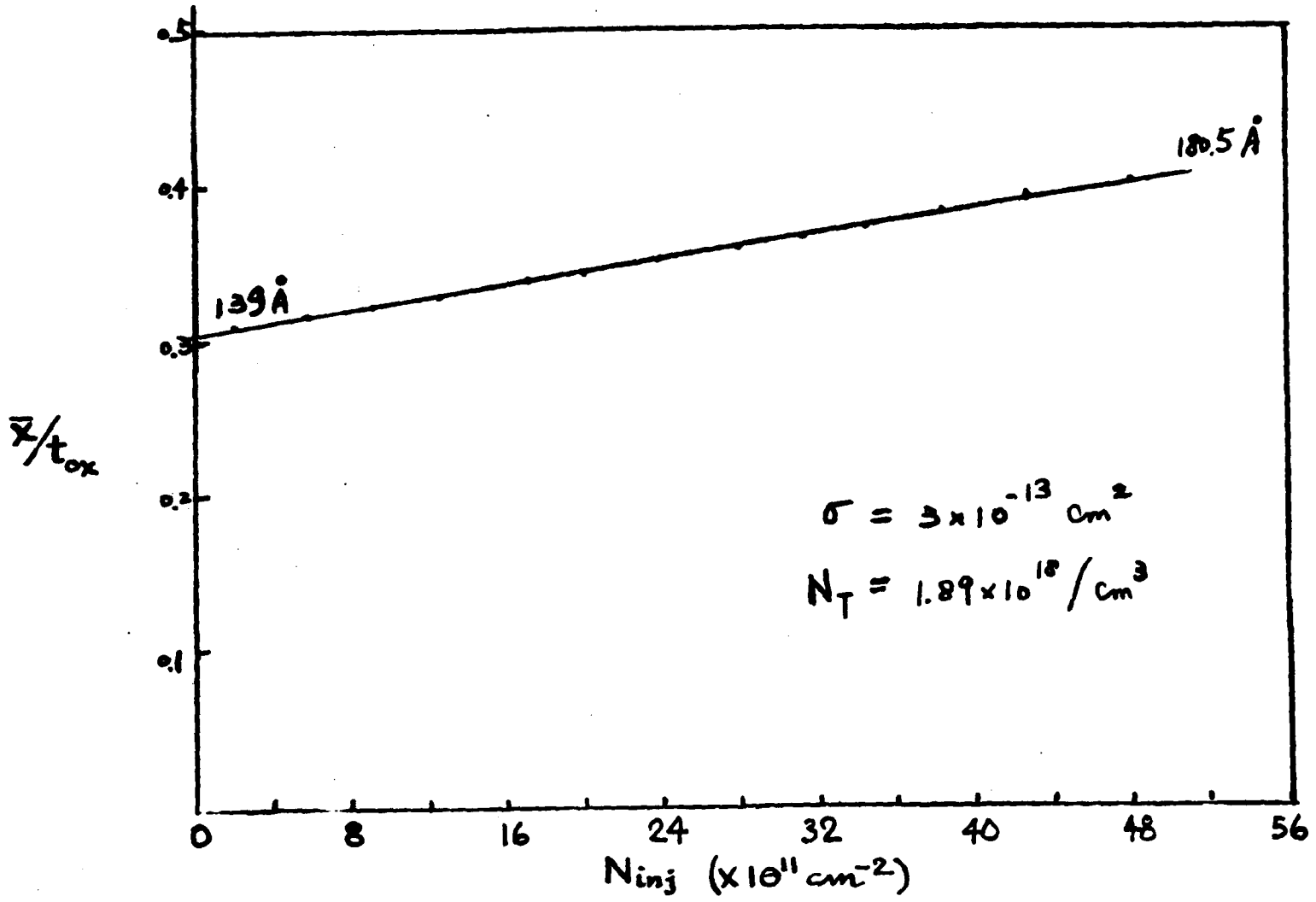

Fig. 5.4. Calculated position of centroid vs N_{inj}.

leads us to believe that impact ionization is not the principal source of the trapped holes. The tunneling of holes from the substrate or an out-tunneling of electrons from neutral centers seem to be likely mechanisms. Electron trapping near the negative electrode and hole trapping near the positive electrode can account for the observed decay in current as time goes on.

Under the assumption of uniformly distributed traps and uniform trapping cross sections, we find the electron trap concentration to be 1.9×10^{18} cm^3 in our samples. The electron trapping cross section is found to be 3×10^{-13} cm^2. The magnitude of this cross section makes it appear likely that the traps are coulomb-attractive in nature.

We plan to study the electron injection mechanisms and expect also to investigate the spatial and energy distributions of the captured electrons.

REFERENCES

A. PUBLICATIONS, REPORTS, AND DOCTORAL DISSERTATIONS RESULTING FROM WORK DONE UNDER THIS PROGRAM

1. M. A. Lampert, W. C. Johnson, and W. R. Bottoms, "Study of Electronic Transport and Breakdown in Thin Insulating Films," Semi-Annual Technical Report No. 1 (AFCRL-TR-73-0263), January 1973.

2. M. A. Lampert, W. C. Johnson, and W. R. Bottoms, "Study of Electronic Transport and Breakdown in Thin Insulating Films," Semi-Annual Technical Report No. 2 (AFCRL-TR-74-0076), July 1973.

3. N. M. Johnson, W. C. Johnson, and M. A. Lampert, "Electron Trapping in Ion-Implanted Silicon Dioxide Films on Silicon," Special Report No. 1 (AFCRL-TR-74-0133), January 1974. (This Special Report was based on N. M. Johnson's doctoral dissertation.)

4. W. C. Johnson, M. A. Lampert, and W. R. Bottoms, "Study of Electronic Transport and Breakdown in Thin Insulating Films," Semi-Annual Technical Report No. 3 (AFCRL-TR-74-0229), January 1974.

5. Z. A. Weinberg, W. C. Johnson, and M. A. Lampert, "Determination of the Sign of Carrier Transported Across SiO_2 Films on Silicon."
   (a) Appl. Phys. Lett. 25, 42 (1974).
   (b) Special Report No. 2 (AFCRL-TR-74-0206), April 1974.

6. D. Y. Yang, W. C. Johnson, and M. A. Lampert, "Scanning Electron Micrographs of Self-Quenched Breakdown Regions in Al-SiO_2-(100) Si Structures."
   (a) Appl. Phys. Lett. 25, 140 (1974).
   (b) Special Report No. 3 (AFCRL-TR-74-0278), June 1974.

7. W. C. Johnson and W. R. Bottoms, "Study of Electronic Transport and Breakdown in Thin Insulating Films," Semi-Annual Technical Report No. 4 (AFCRL-TR-74-0574), July 1974.

8. Z. A. Weinberg, "High-Field Transport in SiO_2 Films on Silicon Induced by Corona Charging," Ph.D. Dissertation, Princeton University, Sept. 1974.

9. D. Y. Yang, W. C. Johnson, and M. A. Lampert, "A Study of the Dielectric Breakdown of SiO_2 Films on Si by the Self-Quenching Technique," Special Report No. 4 (AFCRL-TR-74-0516), October 1974. (This Special Report was based on D. Y. Yang's doctoral dissertation.)

10. Z. A. Weinberg, D. L. Matthies, W. C. Johnson, and M. A. Lampert, "Measurement of the Steady-State Potential Difference Across a Thin Insulating Film in a Corona Discharge."
    (a) Special Report No. 5 (AFCRL-TR-74-0315), October 1974.
    (b) Rev. Sci. Instrum. 46, 201 (1975).

11. W. C. Johnson and W. R. Bottoms, "Study of Electronic Transport and Breakdown in Thin Insulating Films," Semi-Annual Technical Report No. 5 (AFCRL-TR-75-0157), January 1975.

12. Brian K. Ridley, "Mechanism of Electrical Breakdown in SiO_2 Films."
    (a) J. Appl. Phys. 46, 998 (1975).
    (b) Special Report No. 6 (AFCRL-TR-75-0182), March 1975.

13. W. R. Bottoms, D. Guterman, and P. Roitman, "Contrast Mechanisms in Electron Beam Images of Interface Structures."
    (a) Special Report No. 7 (AFCRL-TR-75-0267), May 1975.
    (b) J. Vac. Sci. Technol. 12, 134 (1975).

14. W. R. Bottoms and D. Guterman, "Electron Beam Probe Studies of Semiconductor-Insulator Interfaces."
    (a) Special Report No. 8 (AFCRL-TR-75-0326), May 1975.
    (b) J. Vac. Sci. Technol. 11, 965 (1974).

15. N. M. Johnson, W. C. Johnson, and M. A. Lampert, "Electron Trapping in Aluminum-Implanted Silicon Dioxide Films on Silicon," J. Appl. Phys. 46, 1216 (1975).

16. C. T. Shih, "A Study of the Effects of Low-Energy Electron Irradiation on MOS Capacitors," Ph.D. Dissertation, Princeton University, June 1975.

17. D. Y. Yang, W. C. Johnson, and M. A. Lampert, "A Study of the Dielectric Breakdown of Thermally Grown SiO_2 by the Self-Quenching Technique," 13th Annual Proceedings on Reliability Physics (IEEE), p. 10 (1975).

18. Daniel C. Guterman, "Electron-Beam Induced Imaging and Analysis of Internal Structure in the Metal-Insulator-Semiconductor Structure," Ph.D. Dissertation, Princeton University, November 1975.

19. Walter C. Johnson, "Mechanisms of Charge Buildup in MOS Insulators," IEEE Trans. Nucl. Science NS-22, 2144 (Dec. 1975).

20. Z. A. Weinberg, W. C. Johnson, and M. A. Lampert, "High-Field Transport in SiO_2 on Silicon Induced by Corona Charging of the Unmetallized Surface," J. Appl. Phys. 47, 248 (1976).

21. C. C. Chang, "Study of Lateral Nonuniformities and Interface States in MIS Structures," Ph.D. Dissertation, Department of Electrical Engineering, Princeton University, February 1976.

22. H. S. Lee, "High-Field Effects in SiO_2 Films on Silicon," Ph.D. Dissertation, Department of Electrical Engineering, Princeton University, February 1976.

23. Walter C. Johnson, "Study of Electronic Transport and Breakdown in Thin Insulating Films," Final Report, Contract F19628-72-C-0298 (RADC-TR-76-158), May 1976.

24. S. Baidyaroy, M. A. Lampert, B. Zee, and R. U. Martinelli, "Monte Carlo Studies of Hot-Electron Distributions in Thin Insulating Films: I. Constant Mean Free Path and a One-Dimensional Simulation," J. Appl. Phys. 47, 2103 (1976).

25. Walter C. Johnson, "Study of Electronic Transport and Breakdown in Thin Insulating Films," Semi-Annual Technical Report No. 1, Contract DAAG53-76-C-0059 (NVL-0059-001), 1 June 1976.

26. S. Baidyaroy, M. A. Lampert, B. Zee, and R. U. Martinelli, "Monte Carlo Studies of Hot-Electron Distributions in Thin Insulating Films: II. Constant Mean Free Path and Instability."

(a) Special Technical Report No. 1 (NVL-0059-002), 15 November 1976.

(b) J. Appl. Phys. 48, 1272 (1977).

27. Walter C. Johnson, "Study of Electronic Transport and Breakdown in Thin Insulating Films," Semi-Annual Technical Report No. 2, Contract DAAG53-76-C-0059 (NVL-0059-003), 1 December 1976.

28. Peter Roitman, "Electron Beam Interaction With MOS Capacitors," Ph.D. Dissertation, Princeton University, February 1977.

29. C. C. Chang and Walter C. Johnson, "Frequency and Temperature Tests for Lateral Nonuniformities in MIS Capacitors."

(a) Special Technical Report No. 2 (NVL-0059-004).

(b) Accepted for publication by IEEE Trans. Electron Devices.

B. OTHER REFERENCES

30. E. H. Nicollian, C. N. Berglund, P. F. Schmidt, and J. M. Andrews, J. Appl. Phys. 42, 5654 (1971).

31. R. J. Powell and G. F. Derbenwick, IEEE Trans. Nucl. Sci., NS-18, 99 (Dec. 1971).

32. P. S. Winokur and M. M. Sokoloski, Appl. Phys. Lett. 28, 627 (1976).

33. P. S. Winokur, J. M. McGarrity, and H. E. Boesch, Jr., IEEE Trans. Nucl. Sci., NS-23, 1580 (1976).

34. R. C. Hughes, Appl. Phys. Lett., 26, 436 (1975).

35. R. C. Hughes, E. P. EerNisse, and H. J. Stein, IEEE Trans. Nucl. Sci., NS-22, 2227 (1975).

36. H. H. Sandor and B. L. Gregory, IEEE Trans. Nucl. Sci., NS-22, 2157 (1975).

37. J. R. Srour, S. Othmer, O. L. Curtis, and K. Y. Chu, IEEE Trans. Nucl. Sci., NS-23, 1513 (1976).

38. H. E. Boesch, Jr., F. B. McLean, J. M. McGarrity, and G. A. Ausman, Jr., IEEE Trans. Nucl. Sci., NS-22, 2163 (1975).

39. F. B. McLean, G. A. Ausman, Jr., H. E. Boesch, Jr., and J. M. McGarrity, J. Appl. Phys. 47, 1529 (1976).

40. F. B. McLean, H. E. Boesch, Jr., and J. M. McGarrity, IEEE Trans. Nucl. Sci., NS-23, 1506 (1976).

41. E. Harrari, S. Wang, and B. S. H. Royce, J. Appl. Phys. 46, 1310 (1975).

42. M. Kuhn, Solid State Electronics, 13, 873 (1970).

43. R. Castagne, C. R. Acad. Sci. (Paris), B267, 866 (1968).

44. A. Goetzberger and J. C. Irvin, IEEE Trans. Elec. Dev., ED-15, 1009 (1968).

45. D. M. Brown and P. V. Gray, J. Electrochem. Soc., 115, 760 (1968).

46. P. V. Gray, IEEE Proceedings, 57, 1543 (1969).

47. P. V. Gray and D. M. Brown, Appl. Phys. Lett., 8, 31 (1966).

48. H. E. Boesch, Jr. and J. M. McGarrity, IEEE Trans. Nucl. Science, NS-23, 1520 (1976).

49. C. T. Sah, IEEE Trans. Nuclear Science, NS-23, 1563 (1976).

50. D. M. Brown and P. V. Gray, J. Electrochem. Soc. 115, 760 (1968).

51. A. Goetzberger and J. C. Irwin, IEEE Trans. Electron Devices ED-15, 1009 (1968).

52. W. Shockley and W. T. Read, Phys. Rev. 87, 835 (1952).

53. M. Lax, Phys. Rev. 119, 1502 (1960).

54. R. C. Hughes, Phys. Rev. Letters 35, 449 (1975).

55. T. H. Ning and H N. Yu, J. Appl. Phys. 45, 5373 (1974).

56. K. O. Jeppson and C. M. Svensson, J. Appl. Phys. 48, 2004 (1977).

57. B. E. Deal, M. Sklar, A. S. Grove, and E. H. Snow, J. Electrochem. Sco. 114, 266 (1967).

58. A. Goetzberger, A. O. Lopez, and R. J. Strain, J. Electrochem. Soc. 120, 90 (1973).

59. R. J. Powell and G. F. Derbenwick, IEEE Trans. Nucl. Sci. NS-18, 99 (Dec. 1971).

60. D. J. DiMaria, F. J. Feigl, and S. R. Butler, Phys. Rev. B,11, 5023 (1975).

61. Y. Ota and S. R. Butler, J. Electrochem. Soc. 121, 1107 (1974).

62. T. H. Ning, C. M. Osburn, and H. N. Yu, Appl. Phys. Lett. 26, 248 (1975).

63. T. H. Ning, J. Appl. Phys. 47, 3203 (1976).

64. J. M. Aitken and D. R. Young, J. Appl. Phys. 47, 1196 (1976).

65. J. M. Aitken, D. J. DiMaria, and D. R. Young, IEEE Trans. Nucl. Sci. NS-23 1526 (1976).

66. E. Harari, Appl. Phys. Lett. 30, 601 (1977).

67. T. H. Ning, C. M. Osburn, and H. N. Yu, Appl. Phys. Lett. 29, 198 (1976).

68. T. H. Ning, C. M. Osburn, and H. N. Yu, J. Electronic Materials 6, 65 (1977).

69. H. Harari and B. S. H. Royce, IEEE Trans. Nucl. Science, NS-20, 280 (Dec. 1973).

70. R. J. Powell, Appl. Phys. Lett. 28, 643 (1976).

71. R. J. Powell, J. Appl. Phys. 47, 4598 (1976).

72. T. Tsujide, Jap. J. Appl. Phys. 11, 62 (1972).

73. F. L. Schuermeyer, C. R. Young and J. M. Blasingame, J. Appl. Phys. 39, 1791 (1968).

74. C. N. Berglund and R. J. Powell, J. Appl. Phys. 42, 573 (1971).

75. R. J. Powell, IEEE Trans. on Nucl. Sci. NS-22, 2240 (1975).

76. Noble M. Johnson, private communication.

77. T. H. Ning, J. Appl. Phys. 47, 1079 (1976).

78. P. C. Arnett and B. H. Yun, Appl. Phys. Lett, 26, 94 (1975).

79. A. Mehta, S. R. Butler, and F. J. Feigl, J. Appl. Phys. 43, 4631 (1972).

80. J. W. Tuska and M. H. Woods, Proc. 10th Annual Reliability Physics Symposium, 120 (1972).

81. M. Nakagiri, Jap. J. Appl. Phys. 13, 1610 (1974).